

DISEASES AND DISORDERS

NU6300 covalently reacts with cysteine-191 of gasdermin D to block its cleavage and palmitoylation

Xueqin Jiang^{1†}, Xinlu Zhang^{1†}, Xiaoying Cai^{1†}, Na Li^{1†}, Hongyu Zheng², Minghai Tang¹, Jiangli Zhu³, Kaiyue Su¹, Ruijia Zhang¹, Neng Ye¹, Jing Peng¹, Min Zhao⁴, Wenshuang Wu^{5*}, Jianhong Yang^{1*}, Haoyu Ye^{1*}

Gasdermin D (GSDMD) serves as a vital mediator of inflammasome-driven pyroptosis. In our study, we have identified NU6300 as a specific GSDMD inhibitor that covalently interacts with cysteine-191 of GSDMD, effectively blocking its cleavage while not affecting earlier steps such as ASC oligomerization and caspase-1 processing in AIM2- and NLRC4-mediated inflammation. On the contrary, NU6300 robustly inhibits these earlier steps in NLRP3 inflammasome, confirming a unique feedback inhibition effect in the NLRP3-GSDMD pathway upon GSDMD targeting. Our study reveals a previously undefined mechanism of GSDMD inhibitors: NU6300 impairs the palmitoylation of both full-length and N-terminal GSDMD, impeding the membrane localization and oligomerization of N-terminal GSDMD. *In vivo* studies further demonstrate the efficacy of NU6300 in ameliorating dextran sodium sulfate-induced colitis and improving survival in lipopolysaccharide-induced sepsis. Overall, these findings highlight the potential of NU6300 as a promising lead compound for the treatment of inflammatory diseases.

Copyright © 2024 The Authors, some rights reserved; exclusive licensee American Association for the Advancement of Science. No claim to original U.S. Government Works. Distributed under a Creative Commons Attribution NonCommercial License 4.0 (CC BY-NC).

INTRODUCTION

Gasdermin D (GSDMD) is an essential pyroptosis executioner and a member of the gasdermin family, which includes GSDMA, GSDMB, GSDMC, GSDMD, GSDME, and DFNB59 (1, 2). It consists of two domains, the 31-kDa N terminus (GSDMD-N) and the 22-kDa C terminus (GSDMD-C), separated by a linker region (3). The first flexible loop of GSDMD-C, located between GSDMD-N and the linker helix, stretches out and inserts into the GSDMD-N pocket, stabilizing the conformation of the full-length protein (4). Upon activation, inflammatory caspases cleave GSDMD, producing and releasing GSDMD-N and GSDMD-C (3). Meanwhile, full-length GSDMD or N-terminal GSDMD is palmitoylated at cysteine-191 (C191) upon activation (5, 6). Then, palmitoylated GSDMD-N interacts with acidic phospholipids in the inner leaflet of the plasma membrane, forming functional pores with an inner diameter of 10 to 15 nm through oligomerization (3, 7–9). Excessive pore formation leads to compromised plasma membrane integrity, cellular swelling, secretion of interleukin-1 β (IL-1 β) and IL-18, and, ultimately, pyroptotic cell death (10).

The critical role of GSDMD as a pyroptosis executioner has made it a prominent topic in the field of immunology, which has been linked to immune defense and numerous diseases (11). Studies have shown that GSDMD deletion or inhibition notably decreases pyroptosis and remarkably protect mice from sepsis, which is a fatal condition requiring urgent medical solutions (12–14). In addition,

GSDMD acts as an effector of inflammasome signaling and is implicated in several human diseases, including nonalcoholic steatohepatitis (15), cardiovascular disease (16), inflammatory bowel disease (17), type II diabetes (17, 18), rheumatoid arthritis (19), cancer (20, 21), and Alzheimer's disease (22). Consequently, on account of the crucial function of GSDMD in pyroptosis, it has emerged as an ideal and attracting target for therapeutic intervention of inflammasome-driven diseases.

Since GSDMD is a central effector protein in regulating inflammatory diseases (23, 24), there has been substantial interest in developing drugs that directly target GSDMD. Such drugs not only provide critical insights for exploring and establishing previously unknown mechanism for the study of pyroptosis but also offer a promising avenue for clinical studies in various inflammatory diseases. Up to now, three covalent small molecules have been reported to directly target GSDMD: disulfiram (Dis) (14), necrosulfonamide (NSA) (25), and dimethyl fumarate (DMF) (26, 27). These small molecules react with the free thiol group at cysteine-191/192 (C191/192) in GSDMD, thereby blocking pore formation and pyroptosis (14, 25, 26).

In this study, we conducted a screening of small molecules to identify inhibitors of pyroptotic cell death based on lactate dehydrogenase (LDH) release. Intriguingly, we found that NU6300 was a potent inhibitor of pyroptotic cell death, and it could reduce cytokine release and propidium iodide (PI) intake in human monocytes and murine macrophages. Mechanistically, NU6300 covalently modified human C191 in GSDMD to block its cleavage but had no effect on the earlier steps such as apoptosis-associated speck-like protein containing a caspase recruitment domain (ASC) oligomerization and caspase-1 processing in AIM2 and NLRC4 inflammasomes, proving its high selectivity on GSDMD. On the contrary, we observed robust inhibition of NU6300 on earlier steps of NLRP3 inflammasome, implying a feedback inhibition effect on NLRP3 inflammasome when GSDMD was targeted. We found that NU6300 impaired the palmitoylation of both full-length and N-terminal GSDMD, resulting in the subsequent impediment of GSDMD-N membrane localization. Moreover, we demonstrated that NU6300

¹Department of Biotherapy, Cancer Center and State Key Laboratory of Biotherapy, West China Hospital, Sichuan University, Chengdu 610041, China. ²School of Pharmacy, Chengdu Medical College, Chengdu 610500, China. ³Department of Urology, Cancer Center and State Key Laboratory of Biotherapy, West China Hospital, Sichuan University, Chengdu 610041, China. ⁴Laboratory of Metabolomics and Drug-induced Liver Injury, Department of Gastroenterology and Hepatology, Frontiers Science Center for Disease-related Molecular Network, West China Hospital, Sichuan University, Chengdu 610041, China. ⁵Division of Thyroid Surgery, Department of General Surgery and Laboratory of Thyroid and Parathyroid Disease, Frontiers Science Center for Disease-related Molecular Network, West China Hospital, Sichuan University, Chengdu 610041, China.

*Corresponding author. Email: wenshuang_wu@163.com (W.W.); yjh1988@scu.edu.cn (J.Y.); haoyu_ye@scu.edu.cn (H.Y.)

†These authors contributed equally to this work.

administration attenuated the release of proinflammatory cytokines and provided protection in mice models of colitis and sepsis. Collectively, our results identified NU6300 as a pyroptotic inhibitor that directly targeted GSDMD and held great promise as a potential intervention for inflammatory diseases.

RESULTS

Identification of NU6300 as a potent inhibitor of pyroptosis

Pyroptosis, an inflammatory form of programmed cell death triggered by inflammatory stimuli, has emerged as a promising therapeutic strategy for inflammatory diseases (28). In our research, we performed a screening of covalent compound library containing 565 compounds for inhibitors of pyroptotic cell death based on LDH release on lipopolysaccharide (LPS) plus nigericin-induced pyroptosis in THP-1 cells (Fig. 1A and data S1). Among the active compounds, NU6300 (Fig. 1, B and C) exhibited a dose-dependent rescue effect on pyroptosis, with half maximal inhibitory concentration (IC_{50}) values of 0.89 and 0.93 μ M in THP-1 cells and bone marrow-derived macrophages (BMDMs), respectively (fig. S1A). Furthermore, NU6300 blocked cell death driven by AIM2 or NLRC4 inflammasomes (Fig. 1, D and E). Apart from canonical inflammasomes, NU6300 also inhibited the noncanonical inflammasome-mediated pyroptosis in THP-1 cells and BMDMs (Fig. 1F). NU6300 showed better inhibitory effects on pyroptosis in both THP-1 cells and BMDMs compared with known GSDMD inhibitors such as Dis and NSA, as confirmed by LDH analysis (Fig. 1G and fig. S1B). In addition, we verified that NU6300 displayed no effect on necroptosis (Fig. 1H). The pyroptosis inhibition effect of NU6300 was further validated by PI uptake assay (Fig. 1I and fig. S1C) and live cell imaging of THP-1 cells (fig. S1D). Meanwhile, transmission electron microscopy analysis revealed that NU6300 mitigated the characteristic cytoplasmic swelling and plasma membrane rupture associated with pyroptotic cell death (Fig. 1J). Collectively, these findings suggested that NU6300 effectively inhibited pyroptosis triggered by canonical or noncanonical inflammasomes in both human and mouse cells.

Previous studies indicated that NU6300 was a covalent cyclin-dependent kinase 2 (CDK2) inhibitor (29). Thus, we further tested whether NU6300 inhibited pyroptosis through targeting CDK2. We found that another CDK2 inhibitor, CVT-313, did not successfully inhibit pyroptotic cell death induced by nigericin in THP-1 cells (fig. S2A). We then used lentiviral short hairpin RNA (shRNA) to silence CDK2 expression in THP-1 cells (fig. S2, B and C) and observed no pyroptosis inhibition effect in sh-CDK2 THP-1 cells after nigericin treatment (fig. S2D). These results indicated that the rescue effect of NU6300 might be attributed to off-target effects rather than direct inhibition of CDK2 activity.

NU6300 directly interacts with GSDMD

To investigate the potential target of NU6300 in pyroptosis, we performed the drug affinity responsive target stability (DARTS) assay using protein lysates from THP-1 cells. We observed a prominent protected band at around 50 kDa on the Coomassie brilliant blue staining gel in proteolyzed extracts of cells treated with NU6300, indicating a potential interaction with a protein of interest (Fig. 2A). Using shotgun proteomics based on peptide mass fingerprinting and tandem mass spectrometry (MS/MS), we identified this band as the pyroptosis-related protein GSDMD (table S1). To validate this interaction, we performed immunoblot on DARTS samples in

preferred targets (CAP1, NAPRT, TCP1, UMPS, and GSDMD) in biological MS assay, confirming that NU6300 effectively protected GSDMD from protease hydrolyzation (Fig. 2, B to G, and fig. S3A). We observed a similar binding pattern with purified GSDMD (Fig. 2H and fig. S3, B and C). In addition, cellular thermal shift assay (CETSA) and thermal shift assay (TSA) demonstrated that NU6300 markedly and dose-dependently enhanced the thermal stability of GSDMD protein in both THP-1 cell lysates and purified GSDMD protein accompanying increasing temperature (Fig. 2, I and J). Biolayer interferometry (BLI) analysis revealed a specific binding dissociation constant (K_D) value of 29.1 μ M for NU6300 to GSDMD with K_{on} and K_{dis} rates of 1.51×10^3 (1/ms) and 4.39×10^{-2} (1/s) (Fig. 2K), respectively. Overall, these results confirmed that GSDMD was the direct target of NU6300 in pyroptosis.

NU6300 covalently reacts with C191 of GSDMD

A previous report indicated that NU6300 covalently reacted with Lys⁸⁹ of CDK2 through its vinyl sulfone moiety (29). Given that vinyl sulfone is an emerging electrophile capable of covalently reacting with residues such as cysteine or lysine (30, 31), we hypothesized that NU6300 could react covalently with GSDMD. We conducted liquid chromatography MS/MS (LC-MS/MS) to investigate the effect of NU6300 on GSDMD by incubating recombinant human GSDMD protein with NU6300, revealing a modification of C191 (Fig. 3A), which was important for GSDMD oligomerization. In addition, we detected C56 and C268 modification (fig. S4A). Furthermore, a competitive binding assay demonstrated that preincubation with *N*-acetylcysteine (NAC), a highly reactive cysteine residue that can be inactivated by thiol-reactive compounds (32), notably reversed the inhibitory effects of NU6300 on nigericin-induced pyroptosis in THP-1 cells (Fig. 3B), confirming that NU6300 targeted reactive cysteine. As these three cysteines are all located in the N terminus of GSDMD (p30), which can trigger pyroptosis alone, we expressed N-terminal (p30) in human embryonic kidney (HEK)-293T cells for further validation (fig. S4B). Cytotoxicity analysis revealed that NU6300 concentration-dependently ameliorated the pyroptotic cell death triggered by expression of the p30 fragment in HEK-293T cells (fig. S4C). In addition, PI staining demonstrated that treatment with NU6300 led to a notable reduction in cell death in p30-transfected cells (fig. S4D). We conducted further investigation by introducing cysteine-to-alanine mutations in several conserved human cysteines (C38, C56, C191, and C268) within the p30 fragment. Consistent with the previous report (25), it was observed that C191A mutation on the p30 fragment significantly reduced the cell death compared to the vehicle or full-length GSDMD, while C38A, C56A, and C268A mutations had no effect on cytotoxicity (Fig. 3C). In HEK-293T cells expressing p30, p30-C38A, p30-C56A, p30-C268A, and p30-C38A/C56A/C268A fragments, NU6300 reduced pyroptotic cell death, while it showed no notable reduction in cell death in p30-C191A and p30-C38A/C56A/191A/C268A fragments (Fig. 3, C and D). Furthermore, microscale thermophoresis (MST) assay further revealed that NU6300 had no direct binding with GSDMD C191A (fig. S4E). Collectively, C191 is the important site for covalent modification, and the binding of NU6300 to C56 and C268 is nonspecific and does not affect the function of GSDMD. To further verify the binding of NU6300 to C191 and its pyroptosis inhibition, we synthesized compound NU2, which lacked the vinyl group present in the structure of NU6300 (fig. S5, A and B). Compared to NU2, NU6300 and GSDMD inhibitor

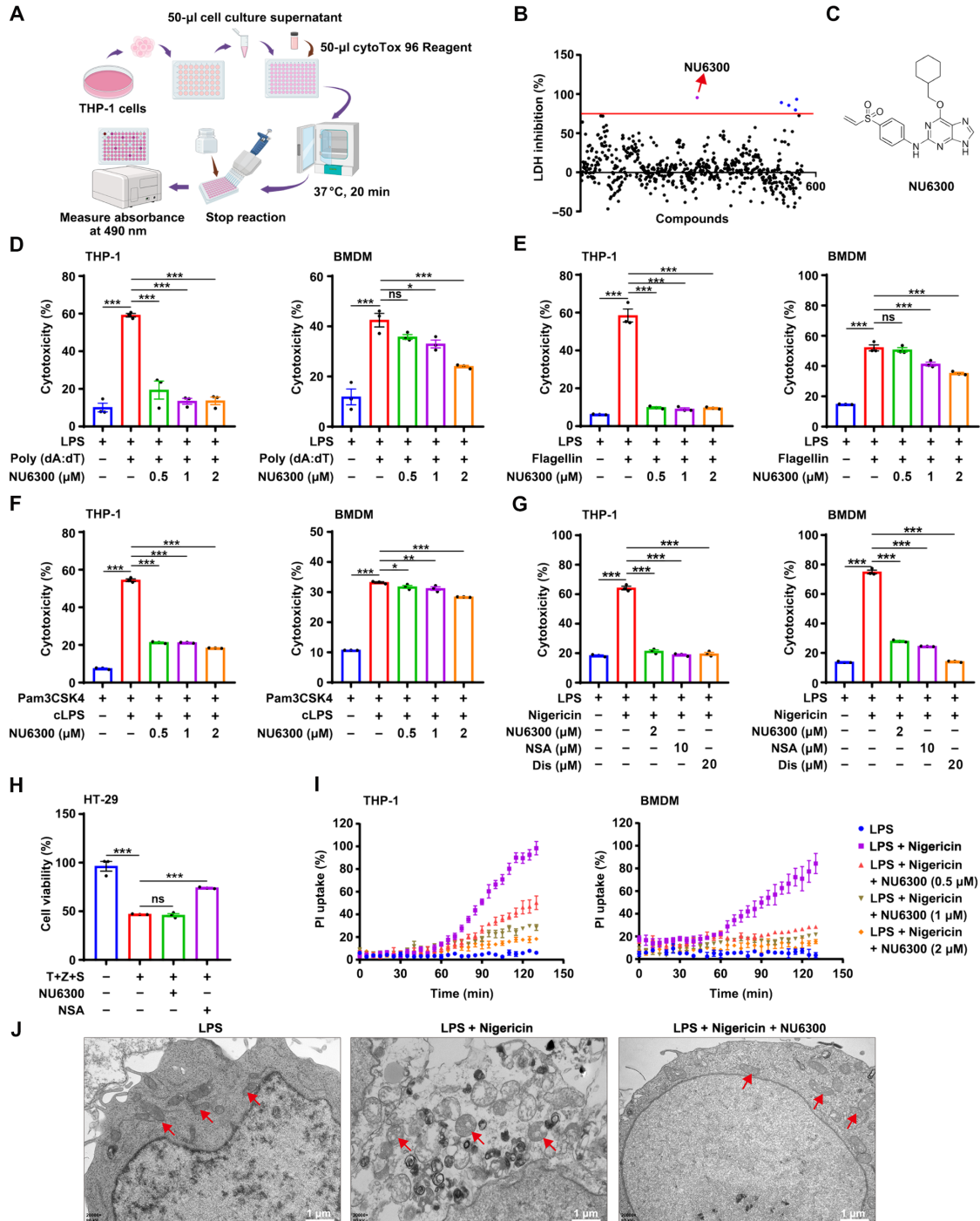


Fig. 1. NU6300 inhibits pyroptosis. (A) Experimental schematic of screening the active small molecules using LDH analysis. (B) THP-1 cells were stimulated with LPS (1 μ g/ml) for 3 hours and then treated with different compounds (2 μ M) for 40 min before they were induced with nigericin (10 μ M) for 35 min, and the inhibition rate of cell death was determined by LDH analysis with a cutoff value of 75% inhibition. (C) Chemical structure of NU6300. (D) and (E) THP-1 cells and BMDMs were primed with LPS and incubated with NU6300 before stimulation with poly(deoxyadenylic-deoxythymidyl acid [poly(dA:dT)] (500 ng/ml) (D) or flagellin (250 ng/ml) (E) for 6 hours, followed by LDH analysis of cell death. (F) THP-1 cells and BMDMs were treated with Pam3CSK4 (400 ng/ml) for 3 hours and incubated with NU6300 before stimulation with cytosolic LPS (1.5 μ g/ml) overnight, followed by LDH analysis of cell death. (G) THP-1 cells and BMDMs were primed with LPS and incubated with NU6300 (2 μ M), NSA (10 μ M), or Dis (20 μ M) before nigericin induction, followed by LDH analysis of cell death. (H) HT-29 cells were pretreated with or without NU6300 (2 μ M) or NSA (10 μ M) for 1 hour before stimulation with TNF α (25 ng/ml) (T), 400 nM SMAC mimetic (S), and 20 μ M z-VAD-fmk (Z) for 24 hours, and cell viability was analyzed by CCK8 assay. (I) Kinetic analysis of PI uptake and cellular membrane permeability after treatment with NU6300 in THP-1 and BMDMs. (J) Transmission electron microscope observation of THP-1 cells morphology. Red arrows indicate representative organelles. Scale bars, 1 μ m. Graphs showed means \pm SEM, $n = 3$. Statistics were analyzed by one-way analysis of variance (ANOVA). * $P < 0.05$, ** $P < 0.01$, and *** $P < 0.001$. ns, not significant.

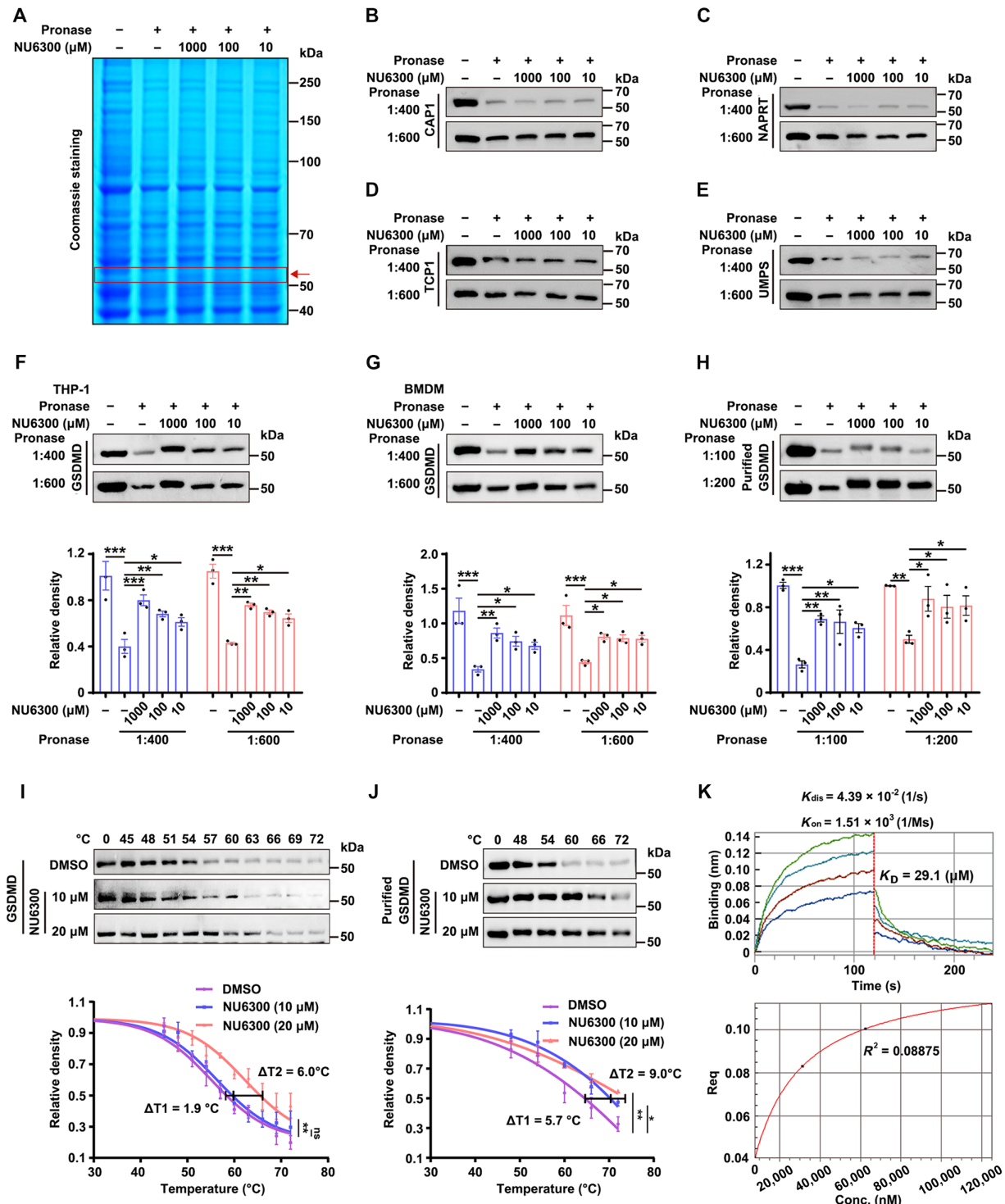


Fig. 2. NU6300 directly interacts with GSDMD. (A) DARTS assay in LPS-primed THP-1 cells treated with dimethyl sulfoxide (DMSO) or NU6300 (1000, 100, and 10 μ M). The lysate samples were digested with pronase (1:500, pronase-to-protein mass ratio) and analyzed by SDS-polyacrylamide gel electrophoresis and Coomassie brilliant blue staining. (B to E) Immunoblot assay to detect the CAP1 (B), NAPRT (C), TCP1 (D), and UMPS (E) proteins by DARTS analysis in LPS-primed THP-1 cells. (F to H) Immunoblot assay to GSDMD protein in THP-1 cells (F), BMDMs (G), and purified protein (H), and the relative density of GSDMD protein was obtained by normalization to the control group. (I and J) CETSA in LPS-primed THP-1 cell lysates (I) or TSA (J) in purified GSDMD protein. The samples were incubated with NU6300 (10 and 20 μ M) at various temperatures, the relative density of GSDMD protein was normalized by the sample without heating, and ΔT_1 and ΔT_2 indicated the thermal shift of NU6300 (10 and 20 μ M) as compared to DMSO control. (K) The binding of GSDMD with NU6300 was evaluated by BLI analysis, and the equilibrium binding signal (Req) was plotted against concentration of analyte. Data were presented as means \pm SEM, $n = 3$. One-way ANOVA or two-way ANOVA was used. * $P < 0.05$, ** $P < 0.01$, and *** $P < 0.001$. ns, not significant.

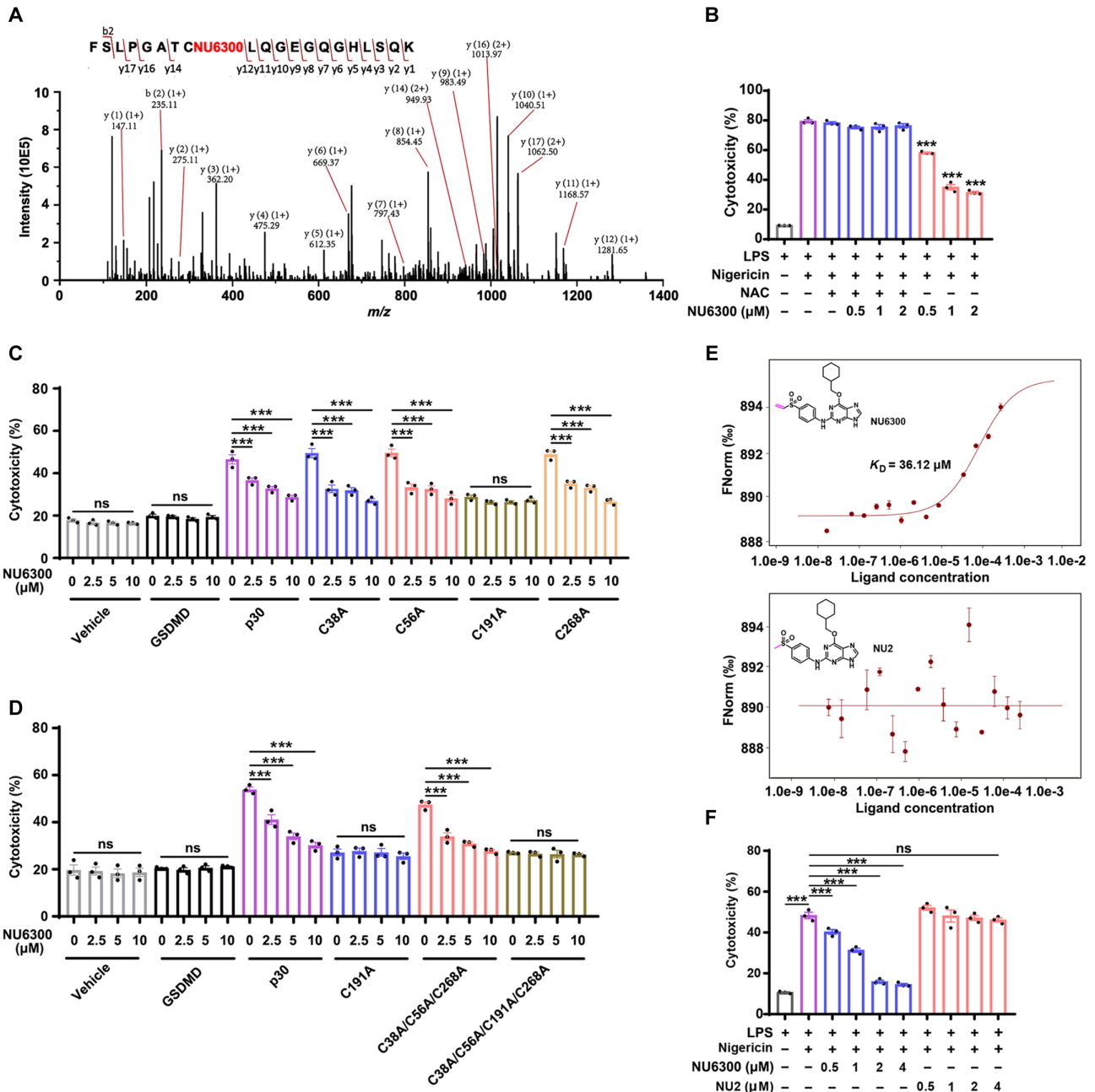


Fig. 3. NU6300 directly binds to C191 of GSDMD. (A) MS/MS spectra of the corresponding human GSDMD peptide FSLPGATCLQGEQQGHLSQK modified on C191 after GSDMD incubation with NU6300. (B) NU6300 (0.5, 1, and 2 μM) and NAC (500 μM) were preincubated for 1 hour before stimulation with nigericin (10 μM) from LPS-primed THP-1 cells for LDH assay. (C) HEK-293T cells were transfected with either GSDMD, p30, p30-C38A, p30-C56A, p30-C191A, or p30-C268A and treated with DMSO or NU6300 (2.5, 5, and 10 μM) before LDH analysis. (D) Inhibitory effect of NU6300 on pyroptosis was evaluated by transfection with GSDMD, p30, p30-C191A, p30-C38A/C56A/C268A, or p30-C38A/C56A/C191A/C268A in HEK-293T cells. (E) MST analysis by incubation of GSDMD protein (0.2 μM) with NU6300 or NU2. (F) Cell cytotoxicity of THP-1 cells was analyzed by stimulation with nigericin and then incubated with NU6300 or NU2 (0.5, 1, 2, and 4 μM). Data were expressed as means \pm SEM, $n = 3$. Comparisons were calculated by one-way ANOVA. *** $P < 0.001$. ns, not significant.

Dis obviously protected against GSDMD degradation in THP-1 cells and BMDMs (fig. S5C). As expected, MST assay further revealed binding of NU6300 to GSDMD with a K_D value of 36.12 μM , whereas no direct binding was observed between GSDMD and NU2 (Fig. 3E); in addition, incubation with NU2 revealed no inhibition of pyroptotic cell death (Fig. 3F). These results strongly indicated that NU6300 directly bound to C191 on GSDMD.

NU6300 blocks the cleavage and palmitoylation of GSDMD

To identify whether NU6300 was selective for GSDMD in inflammasome-GSDMD signals, we investigated the effect of NU6300 on earlier steps. As expected, NU6300 exhibited no or only weak inhibition effect on ASC oligomerization in AIM2, NLRC4, and noncanonical inflammasomes (Fig. 4, A and B, and fig. S6) and no effect on caspase-1 activation in AIM2 and NLRC4

inflammasomes (Fig. 4, C and D), while NU6300 obviously blocked GSDMD cleavage in AIM2 and NLRC4 inflammasomes (Fig. 4, E and F), proving the selectivity of NU6300 on GSDMD.

Recent data demonstrated that palmitoylation of C191 was a requirement for GSDMD membrane translocation and pore formation (5, 6). We further investigated whether NU6300 acted on palmitoylation of GSDMD. As exhibited in Fig. 5 (A to C), NU6300 substantially blocked palmitoylation level of full-length GSDMD in AIM2 and NLRC4 inflammasomes and also obviously inhibited palmitoylation level of GSDMD-N in HEK-293T cells transfected with GSDMD-N. We then extended our investigation into the translocation of GSDMD-N to the membrane in AIM2 and NLRC4 inflammasomes, revealing NU6300's inhibition of GSDMD-N translocation in both inflammasomes (Fig. 5, D and E). However, the conclusion remained elusive because NU6300 concurrently blocked GSDMD cleavage and subsequently reduced N-terminal domain levels. To resolve this ambiguity, we used HEK-293T cells transfected with GSDMD-N to bypass the impact of cleavage. The results corroborated that NU6300 could prevent the GSDMD-N translocation to membrane (Fig. 5F). In addition, NU6300 prominently interrupted the formation of p30 oligomers in HEK-293T cells transfected with GSDMD-N (Fig. 5G). Together, NU6300 covalently modified C191 of GSDMD, blocked its cleavage and palmitoylation, and consequently inhibited GSDMD-N membrane translocation and further oligomerization.

To investigate whether NU6300 was specific to GSDMD-mediated pyroptosis, we also detected its potential binding to other gasdermin family members using DARTS. The results showed that NU6300 failed to protect GSDMA, GSDMB, GSDMC, and DFNB59, except for GSDME (fig. S7, A to E). However, NU6300 did not inhibit GSDME cleavage and GSDME-mediated cell death in etoposide-treated RAW264.7 cells (fig. S7, F to H), indicating that NU6300 did not target GSDME in micromole concentration in cells and the GSDME protection effect of NU6300 on DARTS assay might be a nonspecific result. These results confirmed the selectivity of NU6300 targeting GSDMD over other gasdermin family members.

GSDMD inhibitors show feedback inhibition on NLRP3 inflammasome

NU6300 exhibited a quite strong inhibition effect on earlier steps of NLRP3 inflammasome, with a remarkable inhibition on ASC oligomerization, caspase-1 activation, GSDMD cleavage, membrane translocation, and the release of IL-1 β in nigericin-triggered NLRP3 inflammasome (Fig. 6, A to F). These results impelled us to investigate whether NU6300 also targeted NLRP3 or caspase-1. However, DARTS assay revealed that NU6300 had no protective effect on NLRP3 and caspase-1, and in addition, no direct binding was observed between NU6300 and NLRP3 protein by surface plasmon resonance (SPR) analysis (fig. S8, A to C), indicating no binding of NU6300 to NLRP3 or caspase-1. We further examined the effects of NU6300 and other two known GSDMD inhibitors (NSA and Dis) on earlier steps of the NLRP3 inflammasome–GSDMD signals. All GSDMD inhibitors exhibited noticeable inhibition effects on ASC oligomerization and the cleavage of the pro-caspase-1, pro-IL-1 β , and GSDMD (Fig. 6, G and H). These results suggested that there was a common feedback inhibition effect on NLRP3 inflammasome when GSDMD was inhibited, which was in accordance with previous studies (33, 34).

NU6300 alleviates DSS-induced colitis and LPS-induced sepsis in mice

Aberrant inflammatory responses have been implicated in various pathological conditions, including inflammatory bowel disease and sepsis (35, 36). Activation of GSDMD, a key executioner of pyroptosis, has been observed during intestinal inflammation in a chemically induced colitis model (37). To explore the therapeutic potential of NU6300, we investigated its effect on dextran sulfate sodium (DSS)-induced colitis mouse model. We challenged C57BL/6J mice with 3.25% DSS for 6 days, followed by normal drinking water and concurrent intraperitoneal administration of NU6300 at different doses (5, 10, and 20 mg/kg) or NSA (20 mg/kg) for five consecutive days (Fig. 7A). Notably, NU6300 exhibited a significant dose-dependent mitigation of body weight loss and ameliorated the severity of DSS-induced colitis, as indicated by disease activity index (DAI) scores reflecting body weight loss, diarrhea, and evident rectal bleeding (Fig. 7, B and C). Furthermore, NU6300 administration markedly improved the shortening of the colon length, a characteristic feature of DSS-induced colitis (Fig. 7D and fig. S9A). Meanwhile, histological examination confirmed the beneficial effects of NU6300 on colonic inflammasome, as it mitigated DSS-induced epithelial and mucosal damage, crypt dilation, and goblet cell depletion (Fig. 7E). NU6300 also demonstrated greater efficacy in ameliorating colonic inflammation compared to NSA, a known inhibitor of GSDMD-mediated pyroptosis (38). Both NU6300 and NSA effectively reduced the expression of proinflammatory cytokines IL-1 β and tumor necrosis factor- α (TNF α) by enzyme-linked immunosorbent assay (ELISA) analysis in the colonic area (Fig. 7F) and decreased the level of cleaved caspase-1 and GSDMD protein, as determined by immunoblot analysis (Fig. 7G and fig. S9B). NU6300 greatly improved the severity of DSS-induced colitis compared to NSA administration, suggesting its better therapeutic benefits in ameliorating colitis.

Considering the promising protective effects of GSDMD inhibitors in the LPS-induced mouse model of sepsis (39, 40), we proceeded to assess the potential of NU6300 in this regard. We administered NU6300 (5 and 10 mg/kg) or NSA (10 mg/kg) intraperitoneally to the BALB/c mice for 1 hour before LPS (8 mg/kg) injection (Fig. 7H). Survival analysis showed that mice treated with NU6300 and NSA were effectively protected against the lethal consequences of LPS-induced sepsis (Fig. 7I). After a 4-hour LPS challenge, the NU6300-treated groups exhibited a significant reduction in the concentrations of IL-1 β and TNF α in spleen (Fig. 7, J and K). In addition, spleen from NU6300-treated groups exhibited a significant reduction in spleen index compared to LPS-stimulated mice (Fig. 7L). To check whether the survival protection effect of NU6300 was due to GSDMD inhibition, we compared the survival curves of wild-type and *GSDMD*^{-/-} C57BL/6J mice. *GSDMD*^{-/-} mice were resistant to LPS (50 mg/kg)-induced death as expected, and notably, NU6300 (10 mg/kg) protected wild-type mice from LPS-induced death but did not significantly affect the survival of *GSDMD*^{-/-} mice (Fig. 7M). Moreover, the reduction extent of splenic IL-1 β and TNF α by NU6300 in *GSDMD*^{-/-} mice was not as notable as that in wild-type mice (Fig. 7, N and O), and NU6300 totally lost its pyroptosis inhibition activity in *GSDMD*^{-/-} BMDMs (Fig. 7P). All these results indicated that GSDMD was the main target attributed to the protection effect of NU6300 on sepsis model. However, we noticed that, in *GSDMD*^{-/-} mice, NU6300 also weakly inhibited the expression of splenic TNF α (Fig. 7O), suggesting that there might be other targets of NU6300 accounting for its anti-inflammatory activity.

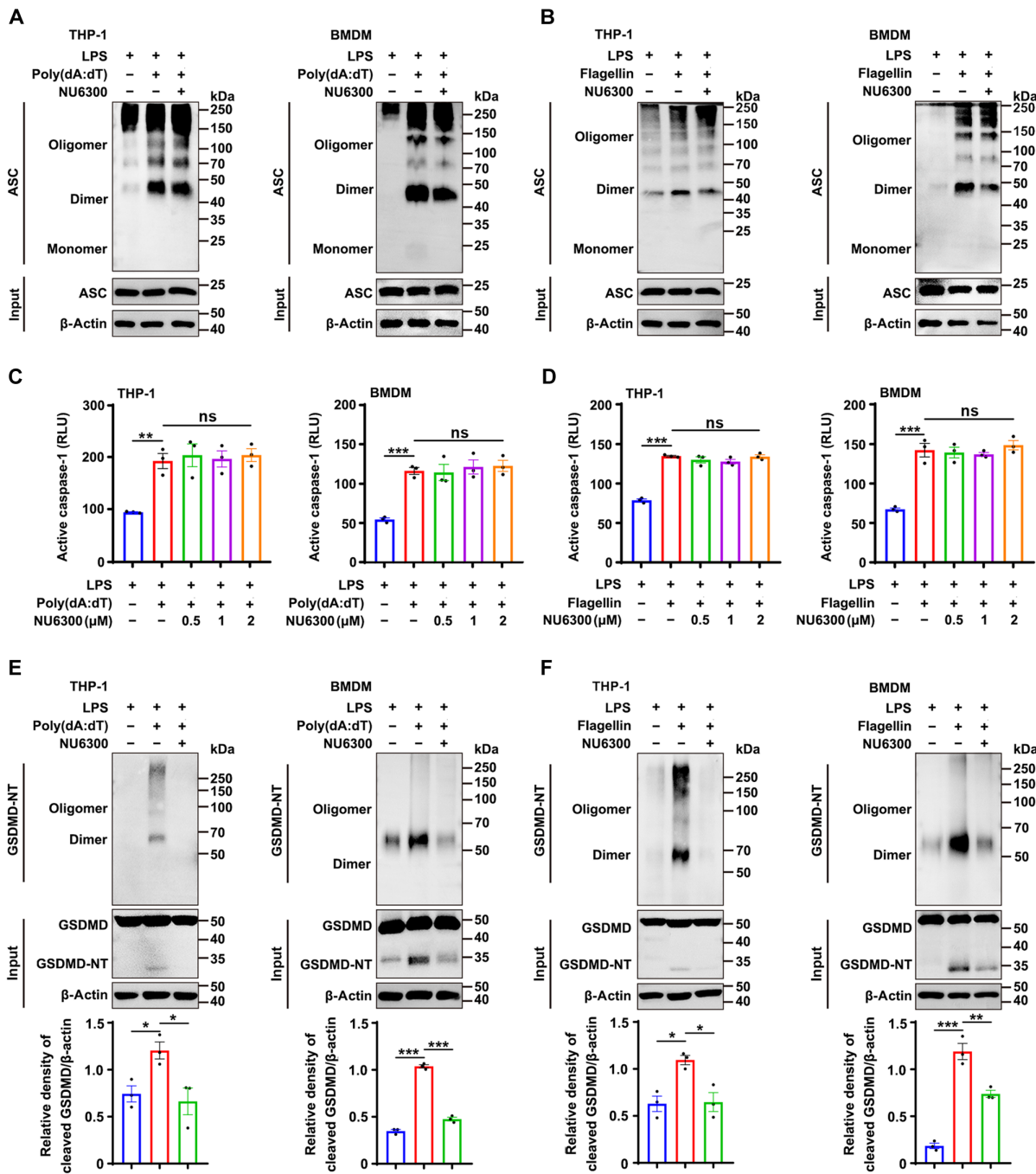


Fig. 4. NU6300 blocks the cleavage of GSDMD. (A and B) ASC oligomerization detection in THP-1 cells or BMDMs by disuccinimidyl suberate cross-linking assays. Cells were primed with LPS (1 μg/ml), incubated with NU6300 (2 μM), and then transfected with poly(dA:dT) (500 ng/ml) (A) and flagellin (250 ng/ml) (B) for 6 hours. (C and D) The caspase-1 activity was measured by Caspase-Glo 1 reagent after AIM2 inflammasome (C) or NLRC4 inflammasome (D) activation in THP-1 cells and BMDMs. (E and F) GSDMD oligomerization and cleavage of GSDMD in THP-1 cells and BMDMs after AIM2 inflammasome (E) or NLRC4 inflammasome (F) activation. Data were expressed as means ± SEM, $n = 3$. Comparisons were calculated by one-way ANOVA. * $P < 0.05$, ** $P < 0.01$, and *** $P < 0.001$. ns, not significant.

Safety and pharmacokinetic properties of NU6300

To evaluate the druggability of NU6300, we first explored potential cardiotoxicity in HEK-293 cells stably transfected with the human ether-a-go-go-related gene (hERG) potassium channel, and NU6300 blocked hERG activity with an IC_{50} of 5.94 μM (fig. S10A). In the maximum tolerated dose (MTD) investigation, we administered

three different doses, namely, 80, 100, and 120 mg/kg. Notably, mice in the 120 mg/kg group experienced fatalities, while the 100 mg/kg group demonstrated a mere deceleration in weight gain, with no incidences of rodent fatalities. Consequently, the MTD of NU6300 in mice was determined to be 100 mg/kg. NU6300 had little effect on heart, spleen, lung, and kidney tissues, except for a weak toxicity

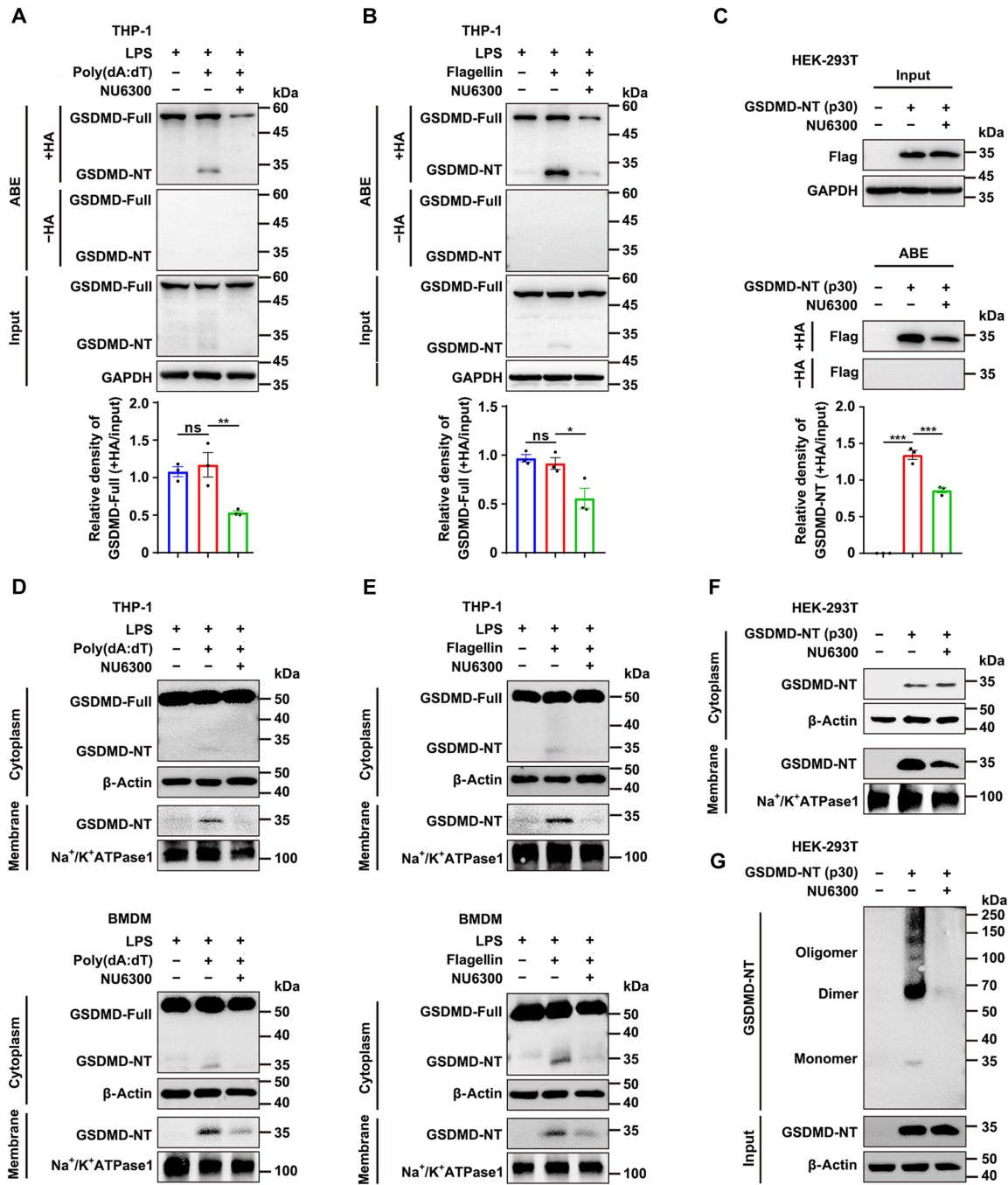


Fig. 5. NU6300 blocks the palmitoylation and membrane translocation of GSDMD-N. (A and B) THP-1 cells were primed with LPS (1 $\mu\text{g}/\text{ml}$) for 3 hours, followed by NU6300 (2 μM), and then transfected with poly(dA:dT) (500 ng/ml) (A) and flagellin (250 ng/ml) (B) for 6 hours, and cell lysates were treated with or without HA and subjected to the acyl-biotin exchange (ABE)–palmitoylation assay. (C) ABE-palmitoylation assay in HEK-293T cells transfected with p30 and incubated with NU6300 (5 μM). (D and E) Expression of GSDMD-NT in cell membrane and cytoplasm after treatment with NU6300 and transfected with poly(dA:dT) (D) or flagellin (E). (F and G) Expression of GSDMD-NT (p30) protein in cell membrane and cytoplasm (F) and the GSDMD-NT oligomerization (G) in HEK-293T cells transfected with p30 and incubated with NU6300 (5 μM). Data were expressed as means \pm SEM, $n = 3$. Comparisons were calculated by one-way ANOVA. * $P < 0.05$, ** $P < 0.01$, and *** $P < 0.001$. ns, not significant.

to the liver, as evidenced by mouse body weight, organ morphology, and organ coefficients (fig. S10, B to D). The 5-day toxicity showed that a slight deceleration in body weight gain and no obvious pathological injury was observed in heart, liver, spleen, lung, and kidney by hematoxylin and eosin (H&E) staining (fig. S10, E and F), implying that NU6300 (20 mg/kg) had no apparent toxicity to vital

organs in vivo. We determined the single-dose pharmacokinetic profile of NU6300 in C57BL/6J mice by administering NU6300 intravenously (20 mg/kg) and intraperitoneally (20 mg/kg). The area under the curve was 137.20 $\mu\text{g} \cdot \text{hour}^{-1} \cdot \text{liter}^{-1}$, with a C_{\max} of 190.09 $\mu\text{g/liter}$ and a half-life of 12.38 hours for intraperitoneal administration (table S2).

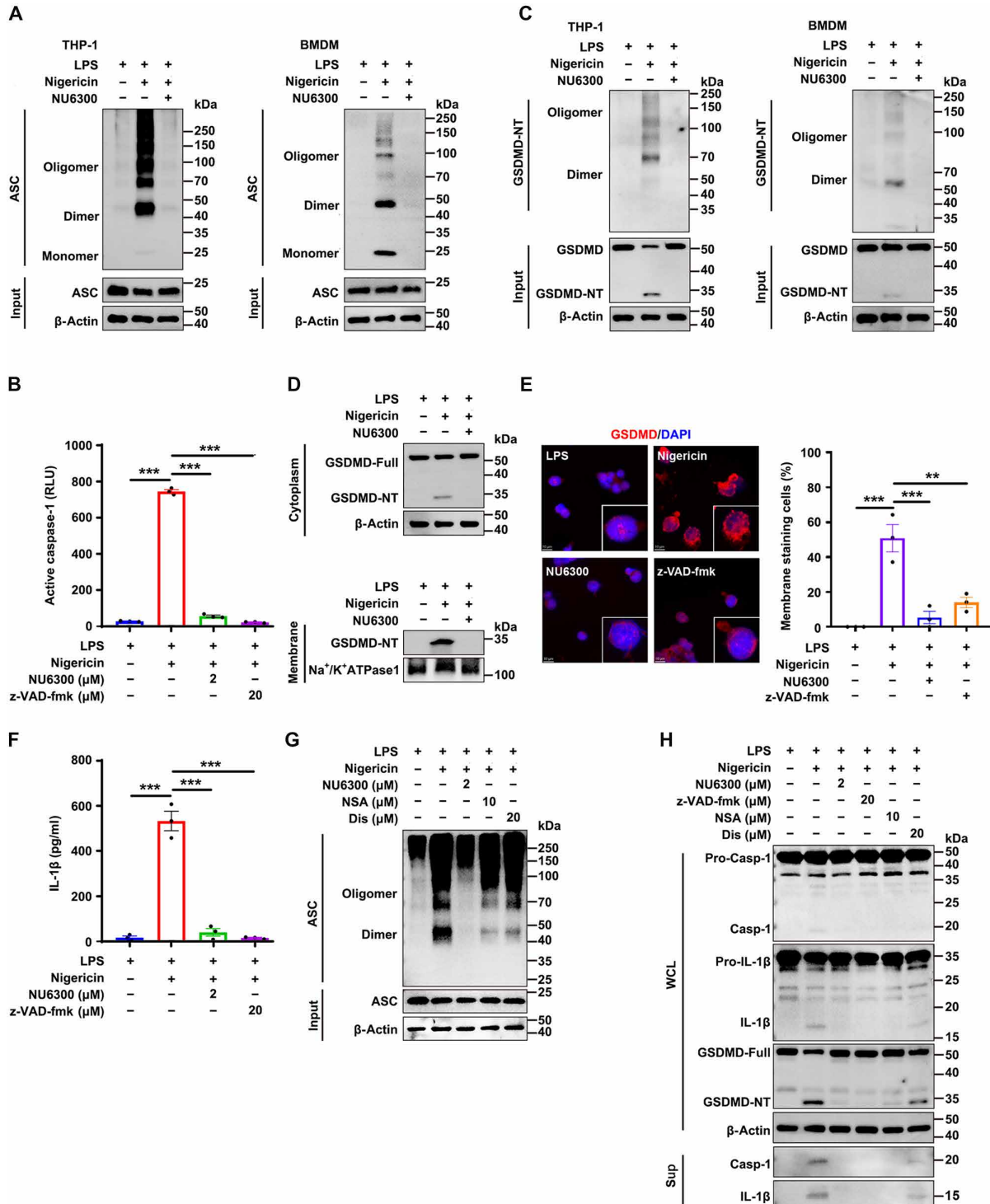


Fig. 6. GSDMD inhibitors show a feedback inhibition on NLRP3 inflammasome. (A) Oligomerization detection by disuccinimidyl suberate cross-linking assays. THP-1 cells and BMDMs were primed with LPS (1 μ g/ml), followed by NU6300 (2 μ M) treatment, and stimulated with nigericin (10 μ M), and then the ASC oligomerization was detected. (B) LPS-primed THP-1 cells were incubated with NU6300 (2 μ M) or z-VAD-fmk (20 μ M) before stimulation with nigericin, and then the caspase-1 activity was measured by Caspase-Glo 1 reagent. (C) The cleavage and oligomerization of GSDMD were analyzed in LPS plus nigericin-activated THP-1 cells and BMDMs. (D) Membrane translocation assay in LPS and nigericin-activated THP-1 cells. (E) Confocal fluorescence microscope study for GSDMD membrane staining after incubation with NU6300 or z-VAD-fmk in LPS plus nigericin-activated THP-1 cells. Scale bars, 10 μ m. (F) The release of IL-1 β was detected by ELISA analysis. (G and H) LPS-primed THP-1 cells were incubated with NU6300 (2 μ M), z-VAD-fmk (20 μ M), NSA (10 μ M), or Dis (20 μ M) before stimulation with nigericin. The treated cells were analyzed for ASC oligomerization (G) and pro-caspase-1, GSDMD, and pro-IL-1 β cleavage, the maturation and release of caspase-1 and IL-1 β (H) by immunoblot of culture supernatants (Sup) or whole-cell lysate (WCL). Graphs showed means \pm SEM, $n = 3$. Statistics were analyzed by one-way ANOVA. ** $P < 0.001$ and *** $P < 0.001$.

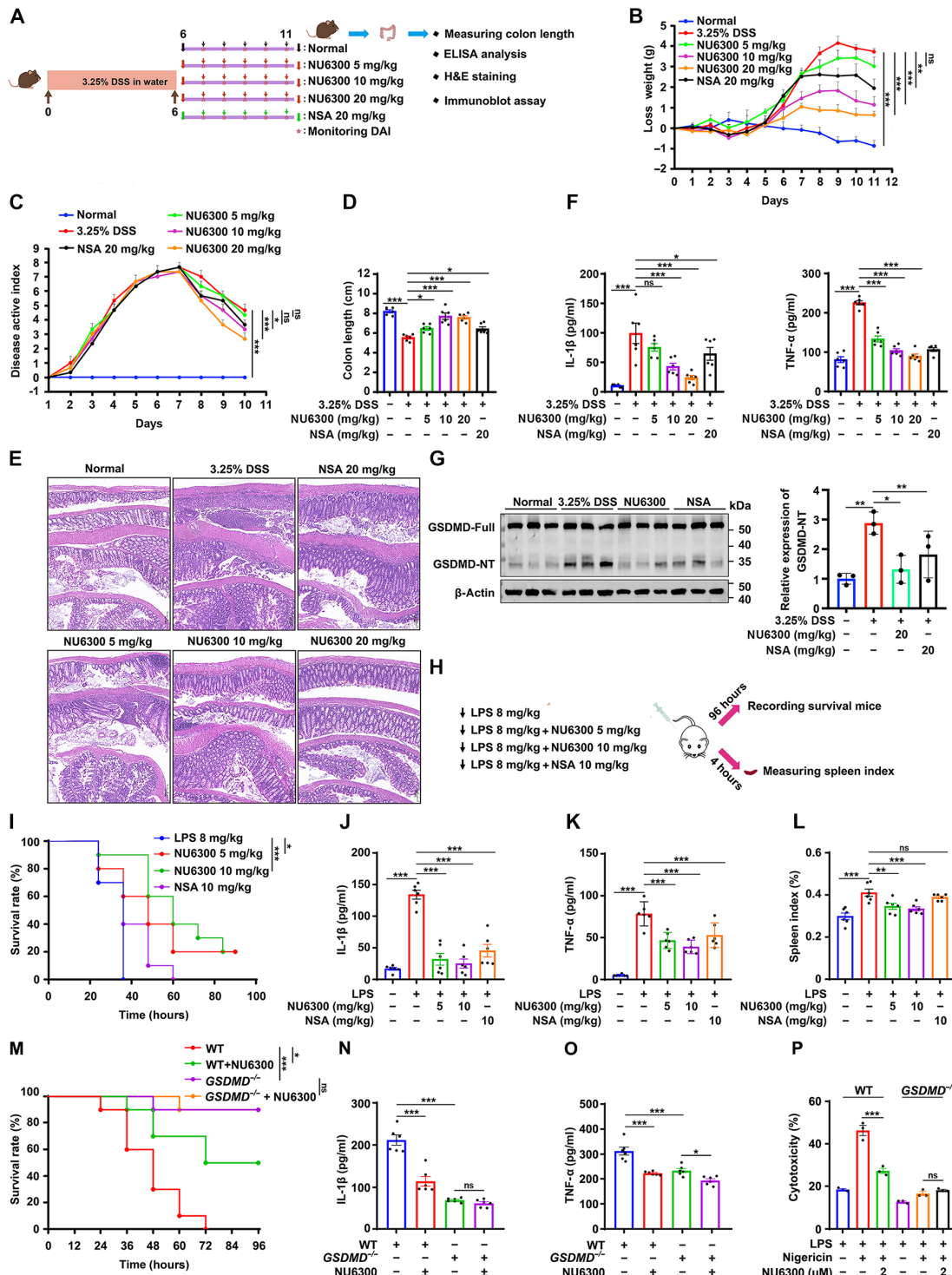


Fig. 7. NU6300 alleviates DSS-induced colitis and LPS-induced sepsis in mice. (A) Flowchart of colitis mouse model induced by DSS (n = 6). (B) Daily loss weight of mice (n = 6). (C) The DAI was recorded (n = 6). (D) Colon length of mice (n = 6). (E) H&E staining to observe the pathological changes of colons. Scale bar, 200 μ m. (F) The IL-1 β and TNF α levels in colon tissues were determined by ELISA analysis (n = 6). (G) The protein expression of cleaved GSDMD in colons was detected by immunoblot assay (n = 3). (H) Flowchart of sepsis mouse model induced by LPS. (I) The survival curves were analyzed after administration with LPS for 4 hours (n = 10). (J to L) Levels of IL-1 β (J) and TNF α (K) in spleen were measured by ELISA, and spleen index (L) was analyzed after administration with LPS for 4 hours (n = 6). (M) Survival curves in wild-type and GSDMD $^{-/-}$ C57BL/6J mice after administration with or without NU6300 (10 mg/kg) for 1 hour and then after challenge with LPS (50 mg/kg) (n = 10). (N and O) Mice were pretreated with or without NU6300 (10 mg/kg) and then injected with LPS (50 mg/kg) for 4 hours, and the levels of IL-1 β (N) and TNF α (O) in spleen were measured by ELISA (n = 6). (P) Cell cytotoxicity of BMDMs in wild-type and GSDMD $^{-/-}$ mice was analyzed by incubation with NU6300 and stimulation with nigericin (n = 3). Data were presented as means \pm SEM, and one-way ANOVA was performed. *P < 0.05, **P < 0.01, and ***P < 0.001. ns, not significant.

Overall, the narrow safety window for cardiotoxicity and low exposure in blood indicated that the druggability of NU6300 was not satisfactory. Further structural optimization was required to enhance its druggability.

DISCUSSION

Dysregulation of inflammation response is centrally incentive in the pathogenesis of various inflammatory diseases, such as sepsis, acute intestinal inflammation, and cancers (35, 41, 42). Recently, a new type of inflammatory programmed cell death, known as pyroptosis, has been found. It is triggered by the activation of canonical and noncanonical inflammasomes, notably via NLRP3 inflammasome activation (1, 43, 44). As GSDMD is a newly identified pyroptosis executioner downstream of inflammasome activation, increasing interest is thus emerging in pursuing GSDMD as a novel therapeutic target for alleviating pyroptosis diseases.

While drug discovery efforts have historically focused on reversibly binding molecules, recent success with covalent inhibitors has highlighted their potential as therapeutic agents (45, 46). Hence, targeted covalent inhibitors have become integral parts of drug discovery approaches (46, 47). NU6300, a CDK2 inhibitor, with vinyl sulfone as the warhead, was identified as a potent inhibitor of pyroptotic cell death. It is the first covalent CDK2 inhibitor with Lys⁸⁹ as the binding site, a residue that lies just outside the CDK2 adenosine triphosphate (ATP)-binding cleft (29). In addition to its involvement in cell cycle regulation, CDK2 was reported as a new target for mitigating neutrophil migration and relieving inflammatory ailments (48). However, we observed no pyroptosis inhibition effect in both noncovalent CDK2 inhibitor CVT-313-treated and CDK2 knockdown THP-1 cells after nigericin induction, indicating that NU6300 might act on other targets to regulate pyroptosis.

DARTS is a universally applicable target identification approach that analyzes direct drug binding to targets (49), which requires no modification of the drug and is independent of any biological effects of the drug (50–52). In our research, we performed DARTS to reveal the potential target of NU6300 account for the anti-pyroptotic effects. Consequently, we identified that GSDMD was the most relevant target. C38, C56, C191, and C268 are four conserved cysteines in the p30 fragment of GSDMD, and NU6300 modified C56, C191, and C268, as indicated by MS data. We thus conducted mutation research on these four cysteines to uncover the potential binding site of NU6300 within p30 fragment. Both single-site and multi-site mutations indicated that C191 was the only modification on GSDMD associated with NU6300's inhibitory effect on pyroptosis. In general, lysine- and cysteine-reactive small molecules might covalently bind to other proteins. However, our research has confirmed that these additional modifications were not relevant to the GSDMD-mediated inflammatory pathway discussed in this study. First, NU6300 suppressed the cleavage, palmitoylation, and subsequent biochemical processes of GSDMD without affecting ASC oligomerization and caspase-1 activation in AIM2 and NLRC4 inflammasomes. This indicated that these additional modifications of NU6300 did not influence the upstream steps. Second, in the mutation experiment, we observed NU6300 deactivation upon GSDMD C191A mutation, providing evidence that the additional modifications of NU6300 did not affect the downstream steps of GSDMD in mediating pyroptosis.

Three reported covalent GSDMD inhibitors, DMF, Dis, and NSA, have different mechanisms of targeting GSDMD (14, 25, 26). Dis and NSA have been reported to inhibit GSDMD oligomerization but with no effect on its cleavage (14, 25), while DMF has been reported to inhibit the interaction between GSDMD and caspase-1, thereby preventing GSDMD cleavage (26). NU6300 inhibited GSDMD cleavage through a mechanism similar to DMF. Recent studies have also shown that reactive oxygen species-dependent palmitoylation of the C191 residue in GSDMD is an important modification for its membrane localization and subsequent oligomerization (5, 6, 53, 54). Our research further demonstrated that NU6300 could remarkably inhibit the palmitoylation of full-length GSDMD and GSDMD-N. In p30-transfected HEK-239T cells, we observed that NU6300 could inhibit the palmitoylation and membrane localization. The palmitoylation-related mechanism has not been reported for existing GSDMD inhibitors, which will have guiding implications for the discovery and mechanistic studies of future GSDMD inhibitors. These studies suggested that NU6300 exhibited a dual-mechanism approach, effectively inhibiting both the cleavage and palmitoylation processes of GSDMD. Palmitoylation could occur on both the full-length GSDMD and GSDMD-N, suggesting that the palmitoylation of GSDMD was independent of its cleavage (5, 6). Furthermore, a specific palmitoylation inhibitor, 2BP, did not inhibit caspase-1-mediated GSDMD cleavage but inhibited LPS and nigericin-induced cell death in a dose-dependent manner (5), indicating that the cleavage of GSDMD was independent of its palmitoylation. This implied that the inhibition of GSDMD cleavage and palmitoylation by NU6300 were two independent mechanisms that contribute to the overall inhibition of pyroptosis. Structurally, NU6300 provided a new skeleton for GSDMD inhibitor that is worthy of further research. However, C191 is located on the edge of GSDMD (55), and there is no protein cavity available for small-molecule binding and design. Therefore, it might be difficult to further design potential compounds based on the aforementioned three small molecules and NU6300. The future research might involve the development of compounds targeting undefined functional sites of GSDMD.

As NU6300 failed to impede the preliminary ASC oligomerization and caspase-1 processing provoked by AIM2 and NLRC4 inflammasome activation, these studies demonstrated that NU6300 displayed selectivity. However, NU6300, together with two known GSDMD inhibitors (Dis and NSA), exhibited strong inhibition effects on NLRP3 inflammasome. These findings revealed a common feedback inhibition effect on NLRP3 inflammasome when GSDMD was inhibited. GSDMD is widely acknowledged as a typical downstream pyroptosis executioner in the NLRP3 inflammasome–GSDMD pathway, while some studies implied that GSDMD might transcend its canonical role by stimulating NLRP3 activation (34). Our results provided solid evidences to support this notion. The underlying mechanism might be explained as follows: When GSDMD was inhibited, the K⁺ efflux was blocked because of abolishment of GSDMD pore-forming capability, which augmented intracellular K⁺ concentration and consequently inhibited NLRP3 activation (56, 57). The feedback inhibition findings suggested that targeting GSDMD might be more effective on NLRP3 than other inflammasomes.

Despite being a covalently irreversible CDK2 inhibitor, no studies have been reported on the efficacy of NU6300 in animal experiments (29). In this study, we evaluated the pharmacological effect of NU6300 on mouse models of colitis and sepsis, given the

well-known role of pyroptosis and IL-1 β release in acute inflammatory bowel diseases and sepsis. As speculated, NU6300 ameliorated the pathology, GSDMD cleavage, and release of inflammatory cytokines associated with acute colitis induced by DSS. Meanwhile, NU6300 reduced the cleavage of caspase-1, indicating that NU6300 primarily acted by limiting feedforward NLRP3 activation and reducing GSDMD pore formation in this model. However, there might also be other mechanisms involved. For instance, NU6300 might directly target upstream signals such as NLRP3 or caspase-1. Nevertheless, our findings revealed no such direct interactions. NU6300 also improved the survival of septic mice and suppressed the release of splenic inflammatory mediators induced by LPS, while it only slightly suppressed the expression of TNF α in GSDMD $^{-/-}$ mice, indicating that GSDMD was the main target attributed to the protection effect of NU6300 on sepsis model and other targets of NU6300 accounting for its anti-inflammatory activity might also be involved.

In summary, our experiments demonstrated that NU6300, an inhibitor of GSDMD, mitigated GSDMD-mediated inflammation both in vitro and in vivo. Mechanistically, NU6300 covalently reacted with C191 of GSDMD to block its cleavage and palmitoylation (Fig. 8). Inhibition of GSDMD held great promise as a therapeutic strategy for inflammatory pyroptosis disorders, and NU6300 represented a promising lead compound for the treatment of inflammatory diseases.

MATERIALS AND METHODS

Plasmids, reagents, and antibodies

Human GSDMD was cloned into a modified pCS2 vector with an N-terminal 3 \times Flag tag for transient expression in HEK-293T cells. All cloning and mutagenesis were verified through DNA sequencing. GSDMD full length (1–484), C-GSDMD (276–484), GSDMD-N/p30 (1–275), p30-C38A, p30-C56A, p30-C191A, p30-C268A, p30-C38A/C56A/C268A, and p30-C38A/C56A/C191A/C268A point mutations were generated by polymerase chain reaction (PCR)-mediated mutagenesis of the cysteine to alanine using KOD Plus Neo DNA polymerase (Toyobo) and subcloning of the mutant cDNAs into the vector using the MonClone Hi-Fusion Cloning Mix V2 kit (Monad, China, Shanghai). For recombinant expression in *Escherichia coli*, the cDNAs were cloned into a modified pET28a vector with an N-terminal 6 \times His-SUMO tag. Truncation mutants of GSDMD were constructed by the standard PCR cloning strategy and inserted into the corresponding vectors. All plasmids were verified by DNA sequencing.

Phorbol 12-myristate 13-acetate (PMA), LPS (serotypes O111: B4 and O55: B5), poly(deoxyadenylic-deoxythymidyllic) acid [poly(dA:dT)], TNF α , and SMAC mimetic were from Sigma-Aldrich. The pan-caspase inhibitor z-VAD-fmk and Dis were from ApexBio. NSA was purchased from TargetMol. Nigericin was obtained from InvivoGen. Flagellin was from Enzo Life Sciences. Caspase-Glo 1 inflammasome assay and CytoTox 96 nonradioactive cytotoxicity assay were from Promega. Lipofectamine 2000 reagent was purchased from Invitrogen. The antibodies adopted in experiments include NLRP3 antibody (Abcam), caspase-1 antibody (p45, p20, AdipoGen), IL-1 β antibody (p31, p17, Affinity), ASC antibody (AdipoGen), GSDMA (Huabio), GSDMB (Abcepta), GSDMC (Huabio), GSDMD antibody (Huabio), GSDME antibody (Abcam), DFNB59 antibody (ImmunoWay), NAPRT (Santa Cruz

Biotechnology), UMPS (Huabio), CAP1(Zen Bioscience), TCP1 (Abways), β -actin antibody (Abways), DDDDK-Tag (Flag, Abclonal), and glyceraldehyde-3-phosphate dehydrogenase (GAPDH) (Abclonal).

Mice

Animal experiments were performed on 8-week-old male C57BL/6J mice (Animal Center of Beijing HFK Bioscience Co Ltd., Beijing, China) and BALB/c mice (Speyford Biotechnology Co. Ltd., Beijing, China). GSDMD knockout mice were purchased from Gempharmatech Co. Ltd. Mice were maintained in specific pathogen-free (SPF)-grade facility and quarantined for a week before the formal experiments. Animal experiments were conducted according to protocols approved by the Animal Care and Use Committees of State Key Laboratory of Biotherapy (Sichuan University).

Cell lines and stimulation

THP-1 cells were cultured in RPMI 1640 (Gibco) supplemented with 10% fetal bovine serum (Procell) and penicillin-streptomycin (100 U/ml; Gibco). BMDMs were obtained from male C57BL/6J mice by culturing in Dulbecco's modified Eagle's medium (DMEM) supplemented with 30% L929 cell culture supernatant for 6 days. HEK-293T cells and HT-29 cells were grown in DMEM with 10% fetal bovine serum and penicillin-streptomycin (100 U/ml).

Differentiated THP-1 cells were acquired by coculturing with PMA (100 ng/ml) for 16 hours, then primed with LPS (1 μ g/ml) for 3 hours, and pretreated with NU6300 (2 μ M) for 40 min before stimulation with nigericin (10 μ M) for 35 min. For AIM2 and NLRC4 inflammasome activation, PMA differentiated cells were primed with LPS and then transfected with poly(dA:dT) (500 ng/ml) or flagellin (250 ng/ml) for 6 hours. For noncanonical inflammasome activation, cells were pretreated with Pam3C-S4K (400 ng/ml) for 3 hours and then stimulated with cytosolic LPS (1.5 μ g/ml). Transient transfection of HEK-293T cells was performed using ExFect Transfection Reagent (Vazyme) according to the manufacturer's instructions. Necroptosis was induced in HT-29 cells by adding TNF α (25 ng/ml) together with 400 nM SMAC mimetic and 20 μ M z-VAD-fmk for 24 hours in the presence or absence of NU6300. Cell viability was determined by CCK8 analysis.

Assays of cell death

Culture supernatants in inflammasome-activated cells were measured by LDH assay according to the manufacturer's instruction. For cytotoxicity in HEK-293T cells, cells were transfected with the plasmid with a complete medium change after 4 hours, followed by NU6300 stimulation for 16 hours before performing LDH determination. To assess cell cytotoxicity and permeability, PI staining assay was conducted. After NU6300 treatment, the cells were cultured in buffered salt solution [25 mM Hepes, 5 mM glucose, 120 mM NaCl, 4 mM KCl, 1.5 mM CaCl₂, 1 mM magnesium chloride, and 0.1% bovine serum albumin (BSA) at pH 7.4] containing PI (2.5 μ g/ml). Maximum fluorescence was measured by lysing each well with 0.1% Triton X-100. Then, the fluorescence at 535/617 nm (excitation/emission) was continuously recorded for 130 min after nigericin activation at 5-min intervals using a Biotek Synergy plate reader, and the images were captured with Nikon microscope. For cell death in RAW264.7 macrophages for GSDME experiments, the cells were plated with 2 \times 10⁵ cells/ml in six-well plate, treated with NU6300

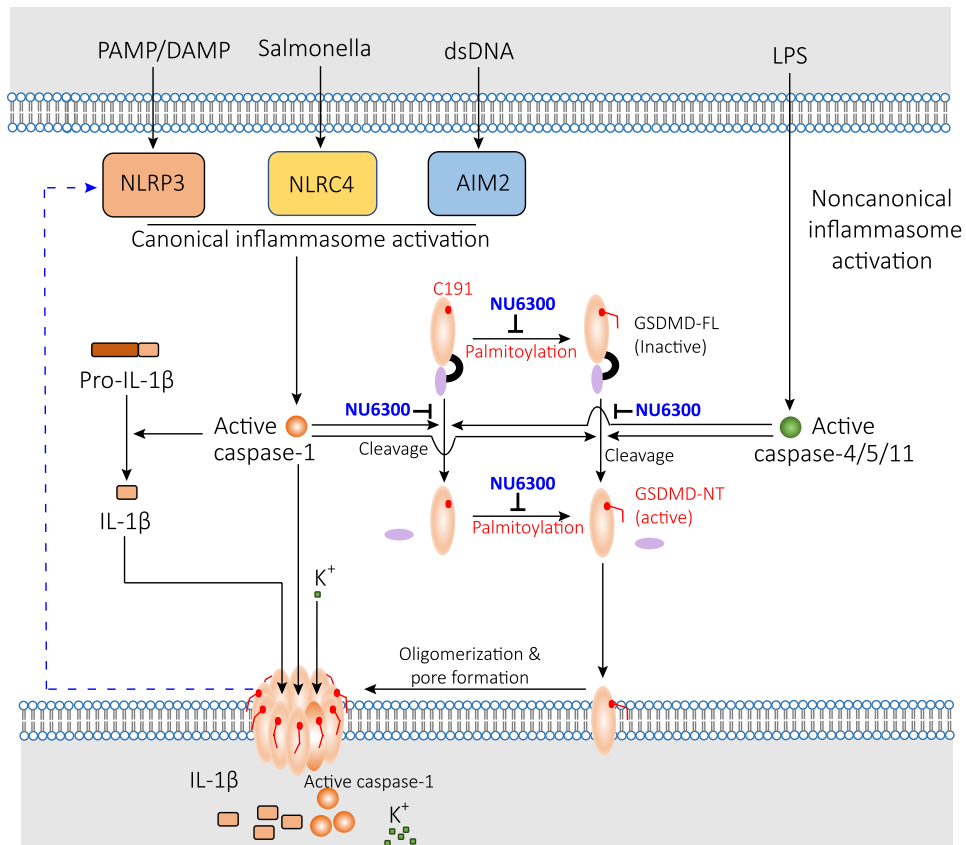


Fig. 8. The mechanism of NU6300 modulating pyroptosis.

for 3 hours, and then stimulated with etoposide (100 μ M) for 16 hours for GSDME-mediated cell death.

Transmission electron microscopy

LPS priming PMA-differentiated THP-1 cells were treated with NU6300 (2 μ M) for 40 min and then induced by nigericin (10 μ M) for 35 min. After incubation, the cells were washed with phosphate-buffered saline (PBS), collected, and then fixed with 0.5% glutaraldehyde at 4°C for 5 min, followed by centrifugation at 12,000 rpm for 15 min. Next, the cell precipitate was fixed in 3% glutaraldehyde. Ultrathin sections were imaged under a JEM-1400PLUS transmission electron microscope (JEOL Ltd., Tokyo, Japan).

Measurement of cytokines

The concentrations of cytokine IL-1 β in culture supernatants from THP-1 cells, BMDMs, colon and spleen from mice, and TNF α in colon and spleen from mice were quantified by ELISA kit (4A BIOTECH) according to the manufacturer's instruction.

Immunoblot

Medium supernatants from macrophages were precipitated by fixing with ice-cold trichloroacetic acid overnight and dissolved in precooled acetone after centrifugation, followed by centrifugation to obtain supernatant samples. Whole-cell lysates were prepared by lysing cell pellets in radioimmunoprecipitation assay (RIPA) lysis buffer with freshly added protease inhibitors and

clarified by centrifugation. All samples were separated by SDS-polyacrylamide gel electrophoresis (SDS-PAGE) and transferred to polyvinylidene difluoride membranes. Following incubation in the primary antibody, the membranes were incubated in horseradish peroxidase-conjugated secondary antibody (Abways) and signals were captured using a gel imaging system (Shanghai Qinxiang, ChemiScope 3200, China).

DARTS and protein site modification

LPS-priming PMA-differentiated THP-1 cells were harvested and lysed with NP-40 lysis buffer and centrifuged at 13,000 rpm for 15 min at 4°C. The total protein content or purified GSDMD protein (0.2 μ g/ml) was incubated with or without NU6300 (1000, 100, and 10 μ M) for 50 min and then digested with pronase (at the indicated protease to protein ratios) for 30 min, followed by termination by addition of protease inhibitor cocktail for 10 min and 5 \times SDS loading buffer to boil for 10 min at 100°C. The samples were separated via SDS-PAGE and examined by immunoblot analysis. For site modification, we incubated 100 μ l of purified human GSDMD (0.45 mg/ml) with NU6300 at a molar ratio of 1:20 (GSDMD protein:NU6300) at room temperature for 3 hours. The unbound small molecules were removed by transferring the sample to a 10-kDa Ultra-0.5 ultrafiltration tube and rinsed with washing buffer [20 mM tris-HCl (pH 8.0), 300 mM NaCl, and 0.5 mM Tris(2-carboxyethyl)phosphine hydrochloride (TCEP)], centrifuged at 10,000 rpm for 5 min, and repeated three times. The sample was collected for SDS-PAGE before Coomassie brilliant blue staining.

MS and sample preparation

For identification of proteins or protein site modification by MS, Coomassie brilliant blue-stained gels were excised and cut into 2- to 3-mm-size pieces and transferred into 1.5-ml polypropylene tubes. Cut gels were destained before incubation with 100% acetonitrile (ACN) at room temperature. After lyophilizing the solvent, samples were digested with sequencing-grade trypsin (Promega, 5 ng/μl) for 20 hours and extracted in 60% ACN/0.1% trifluoroacetic acid, followed by lyophilization. The samples were processed for LC-MS/MS analysis with mobile phase consisting of a 0.1% formic acid aqueous solution (liquid A) and a 0.1% formic acid ACN solution (liquid B). The column was balanced by 95% mobile phase A. Samples were loaded onto a Thermo Fisher Scientific EASY trap column (100 μm by 2 cm, 5 μm, 100 Å, C₁₈) and separated by Thermo Fisher Scientific analytical column (75 μm by 25 cm, 5 μm, 100 Å, C₁₈). The gradient elution program was as follows: 0 to 40 min, 5 to 28% B; 40 to 42 min, 28 to 90% B; 42 to 60 min, 90% B (v/v). The samples were separated by capillary high-performance liquid chromatography, and then analyzed by MS using a Q-Exactive mass spectrometer (Thermo Finnigan, San Jose, CA, USA) in positive ion mode under the following conditions: 375 to 1800 mass/charge ratio (*m/z*) precursor ion scan range with a mass resolution of 120,000 at *m/z* 200, MS1 automatic gain control: 4×10^5 , ion implantation time: 50 ms, cycle time 3 s between master scans. The raw data for MS analysis are raw files, and the software MaxQuant 2.0.1.0 is used for library identification and quantitative analysis.

Protein expression and purification

For expression of full-length human GSDMD, *E. coli* BL21 (DE3) cells harboring the GSDMD plasmid (pET28a-6 × His-SUMO vector) were grown in LB medium supplemented with kanamycin (50 μg/ml) at 18°C overnight after induction with 0.4 mM isopropyl-β-D-thiogalactopyranoside (IPTG) when OD₆₀₀ reached 0.8. The cells were harvested by centrifugation (4500 rpm, 15 min, 4°C), ultrasonicated in the buffer [20 mM tris-HCl buffer (pH 8.0), 300 mM NaCl, 5 mM imidazole, 20 mM MgCl₂, 10 mM KCl, 0.5 mM TCEP, 0.1 mM protease inhibitor], and disrupted by high-pressure micro-fluidization on ice and centrifugation (15,000 rpm, 30 min, 4°C) to isolate the supernatant containing the target protein. The supernatant was then incubated with Ni-nitrilotriacetic acid resin for 1 hour at 4°C and then washed with lysis buffer, after which elution was performed in the lysis buffer supplemented with 300 mM imidazole. The eluted protein was subsequently purified using a desalting column and subjected to SUMO tag overnight cleavage at 4°C by the addition of ULP1 protease. Protein was further subjected to a second round of purification. The purified GSDMD protein was further purified using a superdex 200 gel filtration column (GE Healthcare Life Sciences) preequilibrated with 20 mM tris-HCl buffer (pH 8.0), 300 mM NaCl, and 0.5 mM TCEP. The purified GSDMD was concentrated to 10 mg/ml before freezing at -80°C.

CETSA and TSA

For CETSA analysis, the supernatants of LPS-priming PMA-differentiated THP-1 cells or BMDMs lysed in modified RIPA buffer were harvested and incubated with dimethyl sulfoxide (DMSO) or NU6300. The samples were then subjected to controlled heating, with gradually increasing temperatures from 45° to 72°C for 6 min, followed by cooling at room temperature for 3 min. The samples

were resuspended with 5 × SDS loading buffer and boiled for 10 min before SDS-PAGE for immunoblot analysis. In terms of TSA analysis, the purified GSDMD protein was incubated with DMSO or NU6300 and then heated with increasing temperatures from 48° to 72°C for 6 min for subsequent immunoblot analysis as above described.

BLI assay

Biotinylated GSDMD was prepared, and the BLI analysis was performed as previously described (58). Briefly, the GSDMD protein was dissolved in PBS (100 μg/ml) and subjected to biotinylate with EZ-Link NHS-LC-LC-Biotin kit (Thermo Fisher Scientific). Before each assay, streptavidin (SA) biosensors were pre-wetted in double-distilled water to record the baseline. The biotinylated human GSDMD protein was immobilized on SA-coated 96-well plate surface, after which a 200-μl solution containing DMSO or various concentrations of NU6300 diluted by PBS (containing 2.5% DMSO and 0.02% Tween 20) was added to each well. The binding experiment was performed with repeated cycles consisting of four major steps: initial loading, baseline, association, and dissociation. Data collection and analysis were performed by ForteBio Octet (Port Washington, NY, USA).

MST assay

Protein sample was swapped on the desalting column, and the flow-through was collected after the desalting column had been rinsed with 300 μl of labeling buffer and centrifuged three times at 1500g. Then, the protein was covalently attached by fluorescent label dye RED-NHS. NU6300 was diluted to the indicated concentration and incubated with labeled GSDMD protein for 30 min in assay buffer [20 mM tris (pH 8.0), 300 mM NaCl, 0.5 mM TCEP, and 0.5% Tween 20]. The samples were loaded into the Monolith NT.115 capillaries for MST assay. The *K*_D value was calculated using the mass action equation via the MO Affinity Analysis V2.1.3 software.

Oligomerization assay

For oligomerization, the treated cells were lysed in NP-40 lysis buffer and incubated on a shaker for 30 min at 4°C. After centrifugation at 6000g for 15 min, the cell pellets were cross-linked with fresh disuccinimidyl suberate (2 mM) for 30 min at 37°C and pelleted by centrifugation. The pellets were denatured in SDS sample buffer and subjected to SDS-PAGE analysis.

Immunostaining

PMA-differentiated THP-1 cells were seeded on coverslips overnight and primed with LPS, treated with DMSO or NU6300, and then induced with nigericin. Activated cells were fixed with precooled methanol and blocked with 5% BSA, followed by incubation with GSDMD antibody and fluorochrome-conjugated anti-rabbit immunoglobulin G (IgG). The nuclei were counterstained with 4',6-diamidino-2-phenylindole (DAPI), and GSDMD membrane location was observed by using a Leica confocal microscope.

Membrane localization assay

The treated cells were collected, and then cell membrane and cytoplasmic proteins were extracted by a cell membrane protein and cytoplasmic protein extraction kit (Beyotime) in accordance with the manufacturer's instructions.

Acyl-biotin exchange assay

To detect the palmitoylation of GSDMD, treated cells were lysed with RIPA lysis buffer containing protease inhibitor cocktail. One milligram of protein was then incubated with 1% Triton X-100 and final 25 mM *N*-ethylmaleimide for 30 min at 4°C with gentle full-angle rotation and then precipitated with chloroform-methanol. The air-dried pellet was resuspended in buffer (4% SDS, 5 mM EDTA, and 50 mM tris-HCl, pH 7.4) and divided into two aliquots. The two aliquots were incubated with 800 μ l of PBS containing 0.2% Triton X-100 and 4 mM HPDP-Biotin with or without 0.7 M hydroxylamin (HA) through rotation for 2 hours at 25°C and precipitated protein by repeating the chloroform-methanol assay. To purify biotinylated protein, SA-agarose beads were added and incubated at 4°C for 2 hours. Afterward, the beads were washed with PBS containing 150 mM NaCl and 0.1% Triton X-100 to remove any nonspecifically bound proteins. The biotinylated proteins were eluted by 50 μ l of buffer and boiled for SDS-PAGE analysis.

Caspase-1 activity assay

The caspase-1 activity in cultured cells was detected using Caspase-Glo 1 inflammasome assay kit according to the protocol. THP-1 cells were seeded in 96-well plates with 2×10^5 cells/ml, differentiated with PMA overnight, primed with LPS, treated with DMSO or NU6300, and then induced with nigericin. After induction, the culture medium was removed, 100 μ l of Caspase-Glo 1 reagent or YVAD-CHO reagent was added, and the contents were gently mixed. After incubation at room temperature for 1 hour, luminescence was measured using a Biotek Synergy plate reader.

SPR analysis of recombinant protein

Recombinant human NLRP3 (residues 1 to 1036) was acquired from CUSABIO CSB-EP822275HU (A4), diluted to 50 μ g/ml in sodium acetate (pH 4.0), and then immobilized to the Series S Sensor Chip CM5 (BR100530, Cytiva) through amine-coupling chemistry according to the manufacturer's instructions. Flow cell 1 was immobilized without protein to enable reference subtraction in PBST (PBS containing 0.5% Tween 20, 0.5% DMSO), and flow cell 2 was the detection cell. Single-cycle kinetics was performed for the kinetic experiments, and the analyte compounds were prepared using a fivefold increased concentration gradient in PBST. The equilibrium dissociation constant (K_D) was calculated by Biacore T200 (Cytiva, USA) evaluation software.

DSS-induced colitis model in mice

The male C57BL/6J mice weighing 18 to 22 g were randomly divided into six groups ($n = 6$), and the normal group was allowed to drink water freely. The other groups (DSS, NU6300, and NSA treatment groups) were given 3.25% DSS in drinking water (36,000 to 50,000 M_w , Yeasen Biotechnology Co. Ltd., Shanghai) for 6 days, followed by regular drinking water for 5 days. Meanwhile, the treatment groups were intraperitoneally injected with NU6300 (5, 10, and 20 mg/kg) or NSA (20 mg/kg) as the positive group for five consecutive days. Daily weight loss was recorded, and DAI was monitored throughout the experiment based on body weight, stool consistency, and hemoccult. The mice were sacrificed on day 11, and the colons were collected for determination of colon length, H&E staining analysis, cytokine analysis, and immunoblot assay.

LPS-induced model of sepsis in mice

The BALB/c mice were induced by intraperitoneal injection of LPS (8 mg/kg, O55:B5; Sigma-Aldrich, catalog no. L2880) and administered

with NU6300 (5 or 10 mg/kg) or NSA (10 mg/kg). The wild-type and *GSDMD*^{-/-} C57BL/6J mice were induced by intraperitoneal injection of LPS (50 mg/kg) and administered with NU6300 (10 mg/kg). For survival study, mice ($n = 10$ mice per group) were monitored every 12 hours for a period of 96 hours after administration. To measure cytokines ($n = 6$ mice per group), spleen was collected at 4 hours after LPS challenge, and the concentration of cytokine was determined by ELISA analysis. For spleen index, spleen was excised and spleen index was calculated according to the following equation: spleen index (g/g) = weight of spleen/body weight \times 100%.

hERG test

The inhibitory effect of NU6300 on hERG currents was measured in HEK-293 cells stably transfected with hERG potassium channel with patch clamp. The NU6300 was detected at concentrations of 0.3, 1, 3, 10, and 30 μ M, and the positive control terfenadine was set at 0.001, 0.01, 0.1, and 1 μ M.

MTD of NU6300

The C57BL/6J mice were randomly allocated into three treatment groups (80, 100, and 120 mg/kg) with an equal number of male and female mice. After intraperitoneally administering the aforementioned doses, detailed observations were conducted every day including physical appearance, general behavioral activities, body weight, mortality, and any other abnormal symptoms. On the 14th day after administration, organ coefficients analysis was conducted for the MTD group.

In vivo toxicity study of NU6300

To assess the toxicity of NU6300 in vivo, healthy C57BL/6J mice were given NU6300 (20 mg/kg) intraperitoneally, while an equal volume of 0.9% saline was given to the control group. Mice were sacrificed after 5 days of administration. The heart, spleen, liver, kidneys, and lungs were collected for H&E staining.

Pharmacokinetic study

Male BALB/c mice were randomly divided into two groups ($n = 3$) to receive either intravenous (20 mg/kg) or intraperitoneal (20 mg/kg) administration of NU6300. Blood samples (20 μ l each time) were collected from the posterior orbital venous plexus at 5, 15, and 30 min and 1, 2, 4, 6, 8, 10, and 24 hours after administration. Plasma samples were obtained by centrifugation (3500 rpm, 4°C, 15 min), and then the concentration of NU6300 in plasma was determined by LC-MS/MS analysis. Standard curve for NU6300 in plasma was generated by adding various concentrations, including an internal standard, to blank plasma. The Shimadzu LC-30 AD system was used for separation, with a mobile phase of ACN/0.1% formic acid at a flow rate of 0.5 ml/min. All blood samples were centrifuged and quantified using the Shimadzu LC-30 AD system coupled with AB SCIEX 5500 QTRAP mass spectrometer. Pharmacokinetic parameters were calculated using DAS 2.0.

Statistics

Data were expressed as the SEM and performed at least three times. All data summarization, visualization, and statistical analyses were performed using GraphPad Prism v8.1.2 (GraphPad Software, San Diego, CA). One-way analysis of variance (ANOVA) or two-way ANOVA test was used to determine statistical significance, and differences with $P < 0.05$ were considered

significant. All significant values were indicated as follows: * $P < 0.05$, ** $P < 0.01$, and *** $P < 0.001$.

Supplementary Materials

This PDF file includes:

Supplementary Materials and Methods

Figs. S1 to S10

Tables S1 and S2

Legend for data S1

Other Supplementary Material for this manuscript includes the following:

Data S1

REFERENCES AND NOTES

- J. J. Shi, Y. Zhao, K. Wang, X. Y. Shi, Y. Wang, H. W. Huang, Y. H. Zhuang, T. Cai, F. C. Wang, F. Shao, Cleavage of GSDMD by inflammatory caspases determines pyroptotic cell death. *Nature* **526**, 660–665 (2015).
- S. Feng, D. Fox, S. M. Man, Mechanisms of gasdermin family members in inflammasome signaling and cell death. *J. Mol. Biol.* **430**, 3068–3080 (2018).
- J. J. Ding, K. Wang, W. Liu, Y. She, Q. Sun, J. J. Shi, H. Z. Sun, D. C. Wang, F. Shao, Pore-forming activity and structural autoinhibition of the gasdermin family. *Nature* **535**, 111–116 (2016).
- S. Y. Kuang, J. Zheng, H. Yang, S. H. Li, S. Y. Duan, Y. F. Shen, C. N. Ji, J. H. Gan, X. W. Xu, J. X. Li, Structure insight of GSDMD reveals the basis of GSDMD autoinhibition in cell pyroptosis. *Proc. Natl. Acad. Sci. U.S.A.* **114**, 10642–10647 (2017).
- A. Balasubramanian, L. Ghimire, A. Y. Hsu, H. Kambara, X. Liu, T. Hasegawa, R. Xu, M. Tahir, H. Yu, J. Lieberman, H. R. Luo, Palmitoylation of gasdermin D directs its membrane translocation and pore formation in pyroptosis. *bioRxiv* 2023.02.21.529402 [Preprint] (2023). <https://doi.org/10.1101/2023.02.21.529402>.
- G. Du, L. B. Healy, L. David, C. Walker, P. Fontana, Y. Dong, P. Devant, R. Puthenveetil, S. B. Ficarro, A. Banerjee, J. C. Kagan, J. Lieberman, H. Wu, ROS-dependent palmitoylation is an obligate licensing modification for GSDMD pore formation. *bioRxiv* 531538 [Preprint] (2023). <https://doi.org/10.1101/2023.03.07.531538>.
- L. Sborgi, S. Rühl, E. Mulvihill, J. Pipercevic, R. Heilig, H. Stahlberg, C. Farady, D. Müller, P. Broz, S. Hiller, GSDMD membrane pore formation constitutes the mechanism of pyroptotic cell death. *EMBO J.* **35**, 1766–1778 (2016).
- R. A. Aglietti, A. Estevez, A. Gupta, M. G. Ramirez, P. S. Liu, N. Kayagaki, C. Ciferri, V. M. Dixit, E. C. Dueber, Gsdmd p30 elicited by caspase-11 during pyroptosis forms pores in membranes. *Proc. Natl. Acad. Sci. U.S.A.* **113**, 7858–7863 (2016).
- X. Liu, Z. B. Zhang, J. B. Ruan, Y. D. Pan, V. G. Magupalli, H. Wu, J. Lieberman, Inflammasome-activated gasdermin D causes pyroptosis by forming membrane pores. *Nature* **535**, 153–158 (2016).
- J. Lieberman, H. Wu, J. C. Kagan, Gasdermin D activity in inflammation and host defense. *Sci. Immunol.* **4**, eaav1447 (2019).
- C. L. Wang, J. B. Ruan, Mechanistic insights into gasdermin pore formation and regulation in pyroptosis. *J. Mol. Biol.* **434**, 16729 (2022).
- N. Kayagaki, I. B. Stowe, B. L. Lee, K. O'Rourke, K. Anderson, S. Warming, T. Cuellar, B. Haley, M. Roose-Girma, Q. Phung, P. S. Liu, J. R. Lill, H. Li, J. Wu, S. Kummerfeld, J. Zhang, W. P. Lee, S. J. Snijas, G. S. Salvesen, L. X. Morris, L. Fitzgerald, Y. Zhang, E. M. Bertram, C. C. Goodnow, V. M. Dixit, Caspase-11 cleaves gasdermin D for non-canonical inflammasome signalling. *Nature* **526**, 666–671 (2015).
- W. T. He, H. Q. Wan, L. C. Hu, P. D. Chen, X. Wang, Z. Huang, Z. H. Yang, C. Q. Zhong, J. H. Han, Gasdermin D is an executor of pyroptosis and required for interleukin-1 β secretion. *Cell Res.* **25**, 1285–1298 (2015).
- J. J. Hu, X. Liu, S. Y. Xia, Z. B. Zhang, Y. Zhang, J. X. Zhao, J. B. Ruan, X. M. Luo, X. W. Lou, Y. Bai, J. H. Wang, L. R. Hollingsworth, V. G. Magupalli, L. Zhao, H. B. R. Luo, J. Kim, J. Lieberman, H. Wu, FDA-approved disulfiram inhibits pyroptosis by blocking gasdermin D pore formation. *Nat. Immunol.* **21**, 736–745 (2020).
- B. Xu, M. Z. Jiang, Y. Chu, W. J. Wang, D. Chen, X. W. Li, Z. Zhang, D. Zhang, D. M. Fan, Y. Z. Nie, F. Shao, K. C. Wu, J. Liang, Gasdermin D plays a key role as a pyroptosis executor of non-alcoholic steatohepatitis in humans and mice. *J. Hepatol.* **68**, 773–782 (2018).
- L. P. Du, X. Y. Wang, S. Y. Chen, X. G. Guo, The AIM2 inflammasome: A novel biomarker and target in cardiovascular disease. *Pharmacol. Res.* **186**, 106533 (2022).
- K. Bulek, J. Zhao, Y. Liao, N. Rana, D. Corridoni, A. Antanavičiute, X. Chen, H. Wang, W. Qian, W. A. Miller-Little, S. Swaidani, F. Tang, B. B. Willard, K. McCrae, Z. Kang, G. R. Dubyak, F. Cominelli, A. Simmons, T. T. Pizarro, X. Li, Epithelial-derived gasdermin D mediates nonlytic IL-1 β release during experimental colitis. *J. Clin. Invest.* **130**, 4218–4234 (2020).
- S. Lu, Y. R. Li, Z. J. Qian, T. S. Zhao, Z. W. Feng, X. G. Weng, L. L. Yu, Role of the inflammasome in insulin resistance and type 2 diabetes mellitus. *Front. Immunol.* **14**, 1052756 (2023).
- Y. Ling, M. Xiao, Z. W. Huang, H. Xu, F. Q. Huang, N. N. Ren, C. M. Chen, D. M. Lu, X. M. Yao, L. N. Xiao, W. K. Ma, Jinwujiang capsule treats fibroblast-like synoviocytes of rheumatoid arthritis by inhibiting pyroptosis via the NLRP3/CAPSES/GSDMD pathway. *Evid. Based Complement. Alternat. Med.* **2021**, 4836992 (2021).
- R. Yamagishi, F. Kamachi, M. Nakamura, S. Yamazaki, T. Kamiya, M. Takasugi, Y. Cheng, Y. Nonaka, Y. Yukawa-Muto, L. T. T. Thuy, Y. Harada, T. Arai, T. M. Loo, S. Yoshimoto, T. Ando, M. Nakajima, H. Taguchi, T. Ishikawa, H. Akiba, S. Miyake, M. Kubo, Y. Iwakura, S. Fukuda, W. Y. Chen, N. Kawada, A. Rudensky, S. Nakae, E. Hara, N. Ohtani, Gasdermin D-mediated release of IL-33 from senescent hepatic stellate cells promotes obesity-associated hepatocellular carcinoma. *Sci. Immunol.* **3**, eabl7209 (2022).
- C. A. Traughber, G. M. Deshpande, K. Neupane, N. Bhandari, M. R. Khan, M. R. McMullen, S. Swaidani, E. Opoku, S. Muppala, J. D. Smith, L. E. Nagy, K. Gulshan et al., *iScience* **26**, 106076 (2023).
- H. P. Shen, C. Y. Han, Y. Yang, L. Guo, Y. J. Sheng, J. Wang, W. Y. Li, L. P. Zhai, G. H. Wang, Q. B. Guan, Pyroptosis executive protein GSDMD as a biomarker for diagnosis and identification of Alzheimer's disease. *Brain Behav.* **11**, e02063 (2021).
- B. E. Burdette, A. N. Esparza, H. Zhu, S. Z. Wang, Gasdermin D in pyroptosis. *Acta. Pharm. Sin. B* **11**, 2768–2782 (2021).
- X. Liu, S. Y. Xia, Z. B. Zhang, H. Wu, J. Lieberman, Channelling inflammation: Gasdermins in physiology and disease. *Nat. Rev. Drug Discov.* **20**, 384–405 (2021).
- J. K. Rathkey, J. J. Zhao, Z. H. Liu, Y. H. Chen, J. Yang, H. C. Kondolf, B. L. Benson, S. M. Chirieleison, A. Y. Huang, G. R. Dubyak, T. S. Xiao, X. X. Li, D. W. Abbott, Chemical disruption of the pyroptotic pore-forming protein gasdermin D inhibits inflammatory cell death and sepsis. *Sci. Immunol.* **3**, eaat2738 (2018).
- F. Humphries, L. Shmuel-Galia, N. Ketelut-Carneiro, S. Li, B. W. Wang, V. V. Nemmara, R. Wilson, Z. Z. Jiang, F. Khalighinejad, K. Muneeruddin, S. A. Shaffer, R. Dutta, C. Ionete, S. Pesirisid, S. Yang, P. R. Thompson, K. A. Fitzgerald, Vaccination inactivates gasdermin D and blocks pyroptosis. *Science* **369**, 1633–1637 (2020).
- M. D. Kornberg, P. Bhargava, P. M. Kim, V. Putluri, A. M. Snowman, N. Putluri, P. A. Calabresi, S. H. Snyder, Dimethyl fumarate targets GAPDH and aerobic glycolysis to modulate immunity. *Science* **360**, 449–453 (2018).
- S. M. Man, R. Karki, T. D. Kanneganti, Molecular mechanisms and functions of pyroptosis, inflammatory caspases and inflammasomes in infectious diseases. *Immunol. Rev.* **277**, 61–75 (2017).
- E. Anscombe, E. Meschini, R. Mora-Vidal, M. P. Martin, D. Staunton, M. Geitmann, U. H. Danielson, W. A. Stanley, L. Z. Wang, T. Reuillon, B. T. Golding, C. Cano, D. R. Newell, M. E. M. Noble, S. R. Wedge, J. A. Endicott, R. J. Griffin, Identification and characterization of an irreversible inhibitor of CDK2. *Chem. Biol.* **22**, 1159–1164 (2015).
- J. C. Powers, J. L. Asgian, O. D. Ekici, K. E. James, Irreversible inhibitors of serine, cysteine, and threonine proteases. *Chem. Rev.* **102**, 4639–4750 (2002).
- B. D. Mather, K. Viswanathan, K. M. Miller, T. E. Long, Michael addition reactions in macromolecular design for emerging technologies. *Prog. Polym. Sci.* **31**, 487–531 (2006).
- T. Wolfram, M. Schwarz, M. Reuss, K. Lossow, M. Ost, S. Klaus, T. Schwerdtle, A. P. Kipp, N-Acetylcysteine as modulator of the essential trace elements copper and zinc. *Antioxidants* **9**, 1117 (2020).
- S. Kesavardhanula, R. K. S. Malireddi, T. D. Kanneganti, Caspases in cell death, inflammation, and pyroptosis. *Annu. Rev. Immunol.* **38**, 567–595 (2020).
- K. S. G. de Sa, L. A. Amaral, T. S. Rodrigues, A. Y. Ishimoto, W. A. C. de Andrade, L. de Almeida, F. Freitas-Castro, S. S. Batah, S. C. Oliveira, M. T. Pastorello, A. T. Fabro, D. S. Zamboni, Gasdermin-D activation promotes NLRP3 activation and host resistance to leishmania infection. *Nat. Commun.* **14**, 1049 (2023).
- R. Medzhitov, Origin and physiological roles of inflammation. *Nature* **454**, 428–435 (2008).
- F. Van Hauwermeiren, M. Lamkanfi, The NEK-sus of the NLRP3 inflammasome. *Nat. Immunol.* **17**, 223–224 (2016).
- C. M. Ma, D. X. Yang, B. W. Wang, C. Y. Wu, Y. Q. Wu, S. Li, X. Liu, K. Lassen, L. Dai, S. Yang, Gasdermin D in macrophages restrains colitis by controlling cGAS-mediated inflammation. *Sci. Adv.* **6**, eaaz6717 (2020).
- W. C. Yang, K. X. Tao, Y. X. Wang, Y. Z. Huang, C. H. Duan, T. Wang, C. G. Li, P. Zhang, Y. P. Yin, J. B. Gao, R. D. Li, Necrosulfonamide ameliorates intestinal inflammation via inhibiting GSDMD-mediated pyroptosis and MLKL-mediated necroptosis. *Biochem. Pharmacol.* **206**, 115338 (2022).
- R. F. Shao, X. R. Lou, J. F. Xue, D. Y. Ning, G. B. Chen, L. H. Jiang, Review: The role of GSDMD in sepsis. *Inflamm. Res.* **71**, 1191–1202 (2022).
- C. Q. Wu, W. Lu, Y. Zhang, G. Y. Zhang, X. Y. Shi, Y. Hisada, S. P. Grover, X. Y. Zhang, L. Li, B. G. Xiang, J. M. Shi, X. A. Li, A. Daugherty, S. S. Smyth, D. Kirchhofer, T. Shiroishi, F. Shao, N. Mackman, Y. N. Wei, Z. Y. Li, Inflammasome activation triggers blood clotting and host death through pyroptosis. *Immunity* **50**, 1401–1411.e4 (2019).
- K. Schroder, J. Tschoop, The inflammasomes. *Cell* **140**, 821–832 (2010).

42. K. V. Swanson, M. Deng, J. P. Y. Ting, The NLRP3 inflammasome: Molecular activation and regulation to therapeutics. *Nat. Rev. Immunol.* **19**, 477–489 (2019).
43. N. Kayagaki, S. Warming, M. Lamkanfi, L. Vande Walle, S. Louie, J. Dong, K. Newton, Y. Qu, J. F. Liu, S. Heldens, J. Zhang, W. P. Lee, M. Roose-Girma, V. M. Dixit, Non-canonical inflammasome activation targets caspase-11. *Nature* **479**, 117–121 (2011).
44. P. Broz, V. M. Dixit, Inflammasomes: Mechanism of assembly, regulation and signalling. *Nat. Rev. Immunol.* **16**, 407–420 (2016).
45. L. Boike, N. J. Henning, D. K. Nomura, Advances in covalent drug discovery. *Nat. Rev. Drug Discov.* **21**, 881–898 (2022).
46. S. Y. Chen, S. Lovell, S. M. Lee, M. Fellner, P. D. Mace, M. Bogyo, Identification of highly selective covalent inhibitors by phage display. *Nat. Biotechnol.* **39**, 490–498 (2021).
47. K. Bum-Erdene, D. G. Liu, G. Gonzalez-Gutierrez, M. K. Ghozayel, D. Xu, S. O. Meroueh, Small-molecule covalent bond formation at tyrosine creates a binding site and inhibits activation of Ral GTPases. *Proc. Natl. Acad. Sci. U.S.A.* **117**, 7131–7139 (2020).
48. A. Y. Hsu, D. C. Wang, S. Liu, J. Lu, R. Syahirah, D. A. Bennin, A. Huttenlocher, D. M. Umlis, J. Wan, Q. Deng, Phenotypical microRNA screen reveals a noncanonical role of CDK2 in regulating neutrophil migration. *Proc. Natl. Acad. Sci. U.S.A.* **116**, 18561–18570 (2019).
49. B. Lomenick, R. Hao, N. Jonai, R. M. Chin, M. Aghajan, S. Warburton, J. N. Wang, R. P. Wu, F. Gomez, J. A. Loo, J. A. Wohlschlegel, T. M. Vondriska, J. Pelletier, H. R. Herschman, J. Clardy, C. F. Clarke, J. Huang, Target identification using drug affinity responsive target stability (DARTS). *Proc. Natl. Acad. Sci. U.S.A.* **106**, 21984–21989 (2009).
50. Y. F. Zhong, K. Lee, Y. Y. Deng, Y. M. Ma, Y. P. Chen, X. L. Li, C. G. Wei, S. M. Yang, T. M. Wang, N. J. Wong, A. N. Muwonge, E. U. Azeloglu, W. J. Zhang, B. Das, J. C. J. He, R. J. Liu, Arctigenin attenuates diabetic kidney disease through the activation of PP2A in podocytes. *Nat. Commun.* **10**, 45232 (2019).
51. W. Yang, B. Mu, J. You, C. Tian, H. Bin, Z. Xu, L. Zhang, R. Ma, M. Wu, G. Zhang, C. Huang, L. Li, Z. Shao, L. Dai, L. Désaubry, S. Yang, Non-classical ferroptosis inhibition by a small molecule targeting PHB2. *Nat. Commun.* **13**, 7473 (2022).
52. Z. Wang, Y. Sun, F. Lou, J. Bai, H. Zhou, X. Cai, L. Sun, Q. Yin, S. Tang, Y. Wu, L. Fan, Z. Xu, H. Wang, X. Hu, H. Wang, Targeting the transcription factor HES1 by L-menthol restores protein phosphatase 6 in keratinocytes in models of psoriasis. *Nat. Commun.* **13**, 7815 (2022).
53. P. Devant, E. Borsic, E. M. Ngwa, H. Xiao, E. T. Chouchani, J. R. Thiagarajah, I. Hafner-Bratkovic, C. L. Evavold, J. C. Kagan, Gasdermin D pore-forming activity is redox-sensitive. *Cell Rep.* **42**, 112008 (2023).
54. C. L. Evavold, I. Hafner-Bratkovic, P. Devant, J. M. D'Andrea, E. M. Ngwa, E. Borsic, J. G. Doench, M. W. LaFleur, A. H. Sharpe, J. R. Thiagarajah, J. C. Kagan, Control of gasdermin D oligomerization and pyroptosis by the Ragulator-Rag-mTORC1 pathway. *Cell* **184**, 4495–4511.e19 (2021).
55. S. Y. Xia, Z. B. Zhang, V. G. Magupalli, J. L. Pablo, Y. Dong, S. M. Vora, L. F. Wang, T. M. Fu, M. P. Jacobson, A. Greka, J. Lieberman, J. B. Ruan, H. Wu, Gasdermin D pore structure reveals preferential release of mature interleukin-1. *Nature* **593**, 607–611 (2021).
56. Y. S. Xue, D. E. Tuipulotlu, W. H. Tan, C. Kay, S. M. Man, Emerging activators and regulators of inflammasomes and pyroptosis. *Trends Immunol.* **40**, 1035–1052 (2019).
57. D. P. Zheng, T. Liwinski, E. Elina, Inflammasome activation and regulation: Toward a better understanding of complex mechanisms. *Cell Discov.* **6**, 36 (2020).
58. G. T. Heller, F. A. Aprile, T. C. T. Michaels, R. Limbocker, M. Perni, F. S. Ruggeri, B. Mannini, T. Lohr, M. Bonomi, C. Camilloni, A. De Simone, I. C. Felli, R. Pierattelli, T. P. J. Knowles, C. M. Dobson, M. Vendruscolo, Small-molecule sequestration of amyloid-beta as a drug discovery strategy for Alzheimer's disease. *Sci. Adv.* **6**, eabb5924 (2020).

Acknowledgments: We thank E. Kong (Institute of Psychiatry and Neuroscience, Xinxian Medical University) for the palmitoylation research. **Funding:** This study was supported by the National Natural Science Foundation of China (82174077 and 82272647), the Science and Technology Department of Sichuan Province (2023NSFSC1772, 24QYCX0406, and 24NSFSC6854), the Foundation of Sichuan University (2018SCUH0067), and Science and Technology Achievement Transformation Fund of West China Hospital, Sichuan University (CGZH19010). **Author contributions:** Conceptualization: H.Y., J.Y., W.W., X.J., and N.L. Methodology: X.J., X.Z., X.C., N.L., H.Z., M.T., J.Z., and K.S. Investigation: X.J., X.Z., X.C., R.Z., N.Y., J.P., and M.Z. Formal analysis: X.J., X.Z., X.C., and N.L. Visualization: X.J. and W.W. Supervision: H.Y., J.Y., and W.W. **Competing interests:** The authors declare that they have no competing interests. **Data and materials availability:** All data needed to evaluate the conclusions in the paper are present in the paper and/or the Supplementary Materials.

Submitted 26 May 2023

Accepted 8 January 2024

Published 7 February 2024

10.1126/sciadv.adl9284